Precambrian Research 395 (2023) 107153

Contents lists available at ScienceDirect

Precambrian Research

journal homepage: www.elsevier.com/locate/precamres

Paleoproterozoic alkaline-carbonatite magmatism in the convergent tectonic setting: Evidences from 2.07 Ga Dubravinsky complex in the Eastern Sarmatia

Konstantin A. Savko [a], Alexander V. Samsonov [b], Ekaterina B. Salnikova [c], Maria V. Stifeeva [c], Anton B. Kuznetsov [c], Alexander B. Kotov [c], Yuliya O. Larionova [b], Ekaterina H. Korish [a], Alexander N. Larionov [d], Mariya V. Chervyakovskaya [e], Sergey V. Tsybulyaev [a], Nikolay S. Bazikov [a,*]

[a] Voronezh State University, 394018 Universitetskaya Square 1, Voronezh, Russia
[b] Institute of Ore Geology, Petrography, Mineralogy and Geochemistry (IGEM) RAS, 119017 Staromonetniy per 35, Moscow, Russia
[c] Institute of Precambrian Geology and Geochronology, Russian Academy of Sciences (IPGG RAS), 199034, nab. Makarova, 2, Saint-Petersburg, Russia
[d] Centre for Isotope Research, Karpinsky Russian Geological Research Institute (CIR VSEGEI), 199016, Sredniy pr., 74, Saint-Petersburg, Russia
[e] Zavaritskii Institute of Geology and Geochemistry, Ural Branch, Russian Academy of Sciences, 620219 Pochtovyi per. 7, Yekaterinburg, Russia

ARTICLE INFO

Keywords:
Carbonatite
Paleoproterozoic
Kursk block
Geochronology
Isotope systematics

ABSTRACT

The Dubravinsky alkaline-carbonatite complex (ACC) include two relatively large plutons: the arcuate shape Dubravinka pluton and linear Chernyanka pluton intruding the Paleoarchean TTG of the Kursk block of Sarmatia and consisting of three main lithologies: alkaline pyroxenites, carbonatites (together with silicocarbonatites and phoscorites) and syenites (including alkaline granites). The carbonatites and silicocarbonatites are enriched in trace and rare earth elements, which contents vary significantly.

The source for the alkaline pyroxenites and carbonatites could be enriched protoliths from the subcontinental lithospheric mantle, produced by melting and release of fluids from the subducted oceanic slab at c. 2.1 Ga. The primary igneous C and O isotope composition is preserved in the carbonatite: $\delta^{13}C$ (‰ VPDB) = (−4.9) - (−6.4), $\delta^{18}O$ (‰ VSMOW) = (+8.0) – (+9.8). The alkaline granites display well preserved isotope markers of a long-lasting crustal prehistory indicating Paleoarchean source. The syenites have a lesser contribution of Paleoarchean crustal material.

The alkaline pyroxenites and carbonatites are undoubtedly initially igneous rocks that have undergone c. 2.07 Ga-old high-temperature metamorphism. The Dubravinsky ACC is most likely 2.07–2.08 Ga-old, not much older than the metamorphic event. The Dubravinsky ACC has been formed in a suprasubduction setting from both mantle and crustal sources. It is the earliest known carbonatite complex in the World resulted from subduction-collision processes, and the first sign of transition to deep subduction of the modern style.

1. Introduction

Alkaline-carbonatite complexes (ACC) are scarce in the Earth's crust, yet they attract a lot of attention. This is primarily due to their anomalous enrichment in REE, Nb, and other metals, critical for modern industry (Goodenough et al., 2021). Long-term studies have revealed that ACC were formed at different stages of the Earth's geological evolution from the Neoarchean to the present, mainly in two tectonic settings: post-collision and intraplate (Goodenough et al., 2021; Pirajno 2015 and references in them). These tectonic positions provide good preservation of the ACC igneous rocks. In some cases, however, these complexes underwent later tectonic reworking, strongly transforming primary

* Corresponding author.
E-mail addresses: ksavko@geol.vsu.ru (K.A. Savko), samsonov@igem.ru (A.V. Samsonov), e.b.salnikova@ipgg.ru (E.B. Salnikova), stifeeva.maria@yandex.ru (M.V. Stifeeva), antonbor9@mail.ru (A.B. Kuznetsov), akotov@peterlink.ru (A.B. Kotov), geochron@igem.ru (Y.O. Larionova), korish_k@rambler.ru (E.H. Korish), alexander_larionov@vsegei.sp.ru (A.N. Larionov), masha_vuf_91@mail.ru (M.V. Chervyakovskaya), stsybulyaev@bk.ru (S.V. Tsybulyaev), nickolasss@yandex.ru (N.S. Bazikov).

https://doi.org/10.1016/j.precamres.2023.107153
Received 1 June 2023; Received in revised form 12 July 2023; Accepted 25 July 2023
0301-9268/© 2023 Elsevier B.V. All rights reserved.

igneous mineral assemblages of the ACC, thus complicating geochronological and petrogenetic reconstructions. Such problems are met primarily while studying Precambrian ACC, which were affected by large-scale accretionary and collisional tectonics and associated metamorphism (Hurai et al., 2021; Millonig et al., 2012; Monteiro et al., 2020; Tichomirowa et al., 2006). Consequently, the Early Precambrian carbonatite scarcity is possibly disguised by their alteration. Problems of geochronological, isotope-geochemical, and petrological studies of metamorphosed ACC are discussed below, being exemplified by the Dubravinsky alkaline-carbonatite complex in the Kursk block of Sarmatia.

The Dubravinsky ACC's alkaline rocks and carbonatites were first discovered by drilling in the 1980 s. Recent U-Pb isotope analysis (TIMS) of titanite from the carbonatites yielded 2080 ± 13 Ma, which was interpreted as the minimum age limit of their formation (Albekov et al., 2017). Until now, there was no data on element and isotopic geochemistry and U-Pb isotopic age of the rocks' magmatic crystallization. The aim of this paper is to give a description of petrography, elemental and isotope geochemistry, to determine the age of the carbonatite-pyroxenite-syenite association of the Dubravinsky ACC and tectonic setting in the context of the geodynamic evolution of the Kursk Block of Sarmatia in the Paleoproterozoic.

2. Geological setting

The Kursk block of Sarmatia (Fig. 1) consists of the Paleoarchean Kursk–Besedino granulite–gneiss domain and the Mesoarchean Mikhailovsky granite-greenstone terrane, assembled by c. 2.8 Ga collision (Savko et al., 2021a). During 2.7–2.6 Ga, the block was affected by a plume that produced intraplate felsic and mafic magma and, probably, associated with rifting (Savko et al., 2019). In the 2.6–2.1 Ga interval the Kursk block was a stable platform with some sedimentation during an endogenous lull.

In the period of 2.10–2.05 Ga, the Paleoproterozoic platform of the Kursk block underwent intense endogenous reworking with magmatism, rifting, folding, and metamorphism, associated with subduction and collision processes in the Paleoproterozoic Volga-Don and Ingulo-Sevsk orogens framing the Kursk block (Fig. 1). These events eventually formed the structural framework of Eastern Sarmatia.

Alkaline rocks and carbonatites compose two relatively large the Dubravinka pluton and Chernyanka pluton as well as separate small bodies intruding Paleoarchean gneisses (TTG association) of the Kursk-Besedino domain (Fig. 2 a). Though they are overlain by a 170–200 m thick Phanerozoic sedimentary cover, they have been studied in sufficient detail in boreholes for apatite ores. The Dubravinsky alkaline and carbonatites massif is located between the Tim-Yastrebovka and Volotovo Paleoproterozoic riftogenic structures. In plain view, the massif has an arcuate shape (Fig. 2 b). With a very high probability, it is a large fold that frames semicircular northwestern closure of the large Paleoproterozoic Volotovo synform, comprising c. 2.5–2.4 Ga-old metamorphosed siliciclastic-chemogenic sedimentary rocks and BIFs (Savko et al., 2021b). Neighboring bodies of Neoarchean metabasite to the north of the Dubravinsky massif have similar arched shape (Fig. 2 b). The massif is about 10 km as long with width ranging from 200 to 700 m. It plunges steeply (75–80°) to the south towards the center of the structure.

Three main lithologies of the Dubravinka massif are alkaline pyroxenite, carbonatites (together with silicocarbonatite and phoscorite) and syenites (including alkaline granites). These varieties use to alternate, although the alkaline pyroxenite often form small independent bodies at the intrusion exocontact. The host Paleoarchean TTG and migmatites have undergone fenitization and dominantly have aegirine-richterite-albite-microcline compositon.

Westerly of the Dubravinka massif, three linear bodies of the

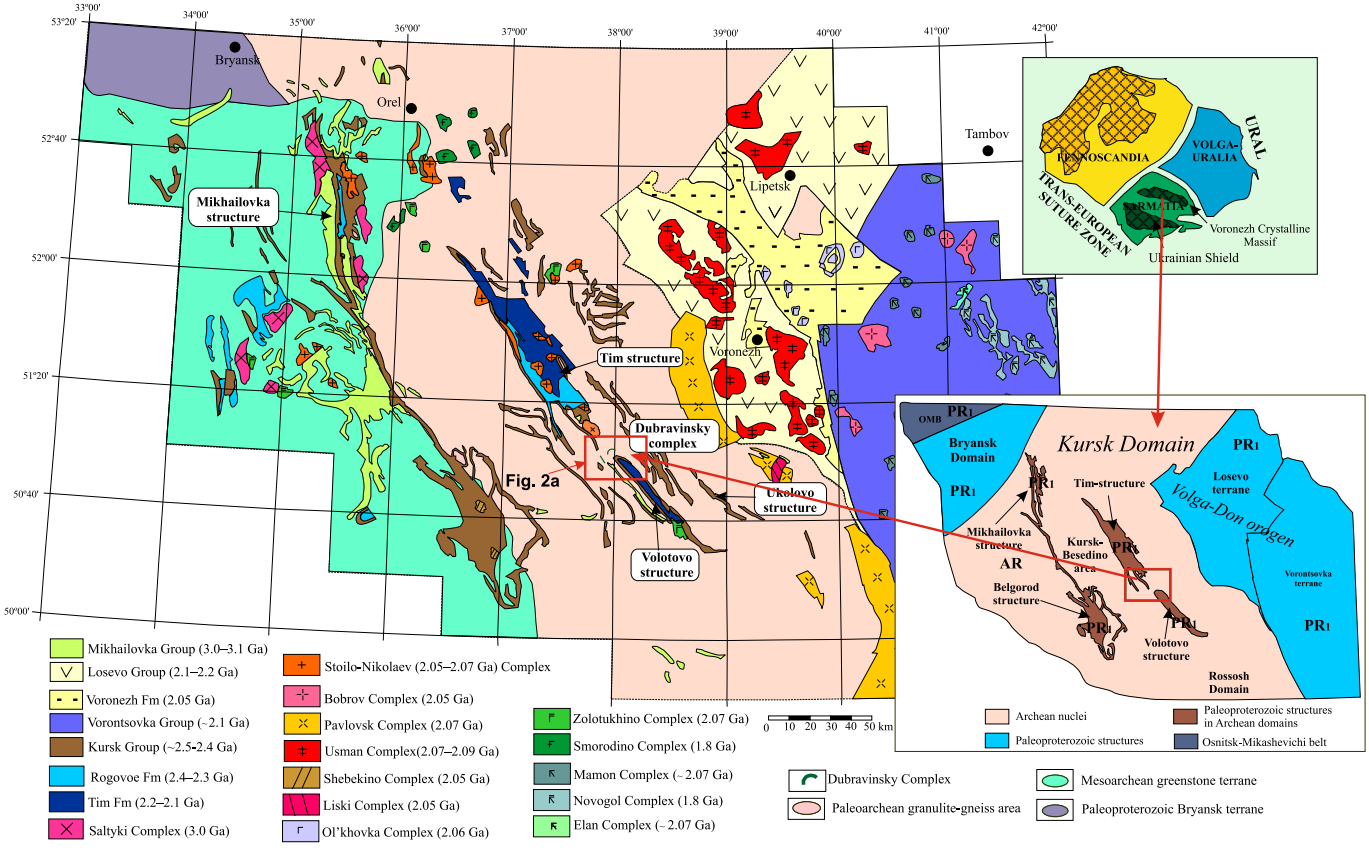

Fig. 1. Schematic geological map of the Voronezh Massif. East European Craton segments after (Gorbatschev and Bogdanova, 1993).

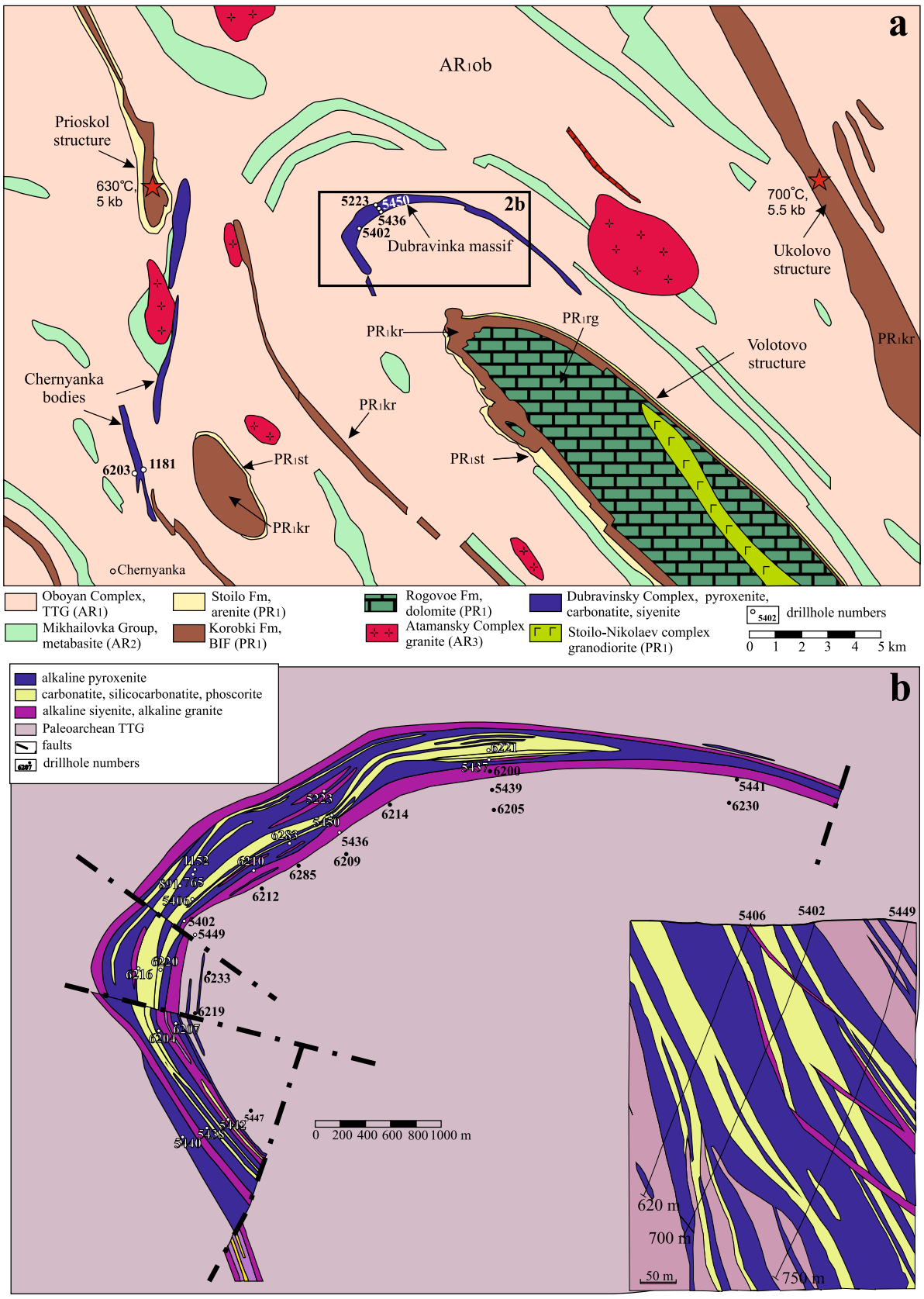

Fig. 2. Schematic geological maps: (a) the Dubravinsky ACC rocks distribution area; (b) the Dubravinka massif and its section.

Chernyanka intrusion consist of alkaline pyroxenites, carbonatites and alkaline granites running in total for c. 7 km from south to north (azimuth 330–340°) at a width of 250–300 m (100–120 m in the southern part), dipping steeply (80° to 90°) to the northeast. Only one borehole 1181 discovered carbonatites closely associating with alkaline pyroxenites: apparently, they are much lesser in volume than in the Dubravinka massif.

3. Geology and petrography of the Dubravinsky alkaline-carbonatite complex

3.1. Carbonatites

The carbonatite compose steeply dipping linear and lenticular bodies, sometimes complexly branching, tens of cm to 10 m (20 m in one case) as thick. Being concentrated in the central part of the massif, they cut the alkaline pyroxenites. No carbonatite are found outside of the alkaline pyroxenite bodies. The thickest carbonatite body contains phoscorites, usually no >2–3 m thick, maximum up to 10 m. There are small injections of carbonatite into alkaline pyroxenites (Supplementary Fig. 1). The carbonatite contain alkaline pyroxenite xenoliths up to 5 × 8 cm in size with biotite rims. The carbonatite, like alkaline pyroxenites, sometimes have directive banded textures.

The carbonatites are greenish-gray to light gray, rarely yellowish-white, fine- to medium-grained (occasionally coarse-grained), with massive, taxite, banded, fluidal, and breccia textures (Supplementary Fig. 1). Their structure is granoblastic, lepidogranoblastic, porphyroblastic with poikillite elements. The carbonatite mineral composition is dominated by calcite (50–90 %). Dolomite (5–10 %), clinopyroxene (3–15 %), richterite (0–10 %), biotite (5–20 %), microcline (0–5 %), titanite (3–10 %), magnetite (2–5 %), and apatite (3–10 %) may also be present (Supplementary Fig. 2). Apart of calcite and dolomite a rare carbonate norsetite [$BaMg(CO_3)_2$] occurs. Accessory minerals are ilmenite, barite, pyrrhotite, galena, molybdenite, monazite, bastnäsite, and zircon. Amount of silicate minerals varies from 10 to 20 to 40–45 %. Clinopyroxene compositionally corresponds to magnesian (X_{Mg} = 0.7–0.9) aegirine-augite with the akmite component of 14 to 50 % (Supplementary Fig. 3). Amphibole is represented by members of the richterite-arfvedsonite isomorphic series. Magnesian biotite (X_{Mg} = 0.71–0.87) often has a deficit of Al_2O_3 and is represented by tetraferri-biotite. Microcline contains up to 3 wt% of BaO. Fluorine-apatite of oval shape (with rounded terminations) typically bears REE at 1–3 wt% level.

With a decrease of carbonates and increase of pyroxene, amphibole, biotite, and titanite, the carbonatites pass into silicocarbonatites usually having a banded texture. The latter is emphasized by variable proportions carbonate and silicate minerals. Therefore, definition of the carbonatites and silicocarbonatites is often arbitrary.

The carbonatites comprise small bodies (up to 1–2 m thick) of phoscorite – a biotite-magnetite-apatite-carbonate rock. They are distinguished from typical phoscorite by absence of olivine. The contacts of phoscorites with clinopyroxenites are sharp, and have 1–2 cm-wide transition zone to the carbonatites. Unlike the carbonatite, apatite in phoscorites has an euhedral shape. Titanite forms numerous small crystals along the edges of large magnetite grains and biotite. Aegirine-augite and richterite may also be present in minor amounts.

3.2. Alkaline pyroxenites

Alkaline pyroxenites occur in the central and marginal parts of the semicircular Dubravinka intrusion and linear Chernyanka intrusion, where they dominate, composing from 70 to 80 % of their volume. They are often intruded by dikes of syenite, carbonatite, and silicocarbonatite and contain dissemination, veinlets, and lenticular segregations of calcite (Supplementary Fig. 1). Contacts with the carbonatite are uneven, sinuous, or embayed.

The alkaline pyroxenites, when unaffected by hydrothermal and metasomatic alterations, are dark green, dark gray, medium and coarse grained rocks with massive, taxitic, and gneissic texture. Their structure is granoblastic and lepidogranoblastic – clearly metamorphogenic. Alkaline pyroxenite consist of 80 % Na-bearing diopside (X_{Mg} = 0.59–0.79) (Supplementary Fig. 3), richterite (up to 15 %), biotite (5–10 %) (Supplementary Fig. 2). Biotite is high-titanium (3–4 % TiO_2) with a noticeable deficiency of Al_2O_3. Sometimes garnet with admixture of TiO_2 (2.2–3.4 wt%) is present. It forms clusters of grains of irregular shape, ocassionally forms euhedral grains of dark brown color. The garnet composition corresponds to andradite (And 85.1 %, Mor 8.1 %, Sch 1.9 %, Gold 0.5 %, Gross 0.4 %, Pyr 0.2 %). The alkaline pyroxenite always contains magnetite, titanite, and apatite, often zircon, ilmenite, and sulfides.

Most of the alkaline pyroxenites are intensively hydrothermally and metasomatically altered during intrusion of carbonatite and syenite. Significant amounts of biotite and microcline appear in them, as well as augens of carbonate, a “carbonate network”, and sometimes peculiar “injections” of carbonatite (Supplementary Fig. 1). In addition, an amphibolite facies metamorphism, apparently accompanied by the renewal of hydrothermal activity, also contributed to changes of their composition and mineralogy, producing widespread microcline alkaline pyroxenite. The latter are coarse-grained rocks with an inequigranular poikillite structure and a taxitic texture due to occurrence of small clinopyroxene crystals clusters in combination with a large microcline laths containing numerous inclusions of clinopyroxene, biotite, titanite, and apatite (Supplementary Fig. 2). Pyroxene is represented by aegirine-augite. In the alkaline pyroxenite’s contact zones with the carbonatite and syenite, predominantly biotite rocks (glimmerites) appear, consisting of biotite (80 %), microcline (5–10 %), carbonate (5–10 %), titanite, apatite and clinopyroxene (5 %).

3.3. Alkaline syenites and granites

Alkaline syenites and granites form dikes 1 to 120 m as thick, cutting the alkaline pyroxenite at angles of 60–80°, carbonatite and host Paleoarchean orthogneisses (TTG); they contain a large amount of xenoliths of the alkaline pyroxenites and carbonatites. They are most widespread at the southeastern flank of the Dubravinka intrusion, where they reach a thickness of tens of meters. Smaller dikes and veins a few meters thick occur everywhere.

The syenite is gray, pink-gray medium- to coarse-grained, with massive and gneissic texture. Unlike the pyroxenites and carbonatites, they retain their primary igneous (allotriomorphic-granular) structure. The syenite is composed of microcline (50–60 %), aegirine or aegirine-augite (10–15 %), biotite (3–5 %), quartz (0–5 %), albite (0–5 %). Accessory minerals are titanite, apatite, zircon, garnet, magnetite, and ilmenite. Reaction zones composed of alkaline amphibole and biotite with apatite and sulfides are observed at the contact of syenites and carbonatites. At contacts with the clinopyroxenite, there are discontinuous biotite-microcline zones and segregations with biotite rims.

The alkaline granite is scarcer than the syenite, forming steeply dipping small dikes, intersecting the alkaline pyroxenite, carbonatite and syenite. Thicker dikes (up to 100 m thick) occur in the syenite in the footwall of the Dubravinka massif, as it has been shown by drilling. The alkaline granite is medium-grained, sometimes porphyric with a granitic structure. In addition to microcline, they contain quartz (15–20 %), albite (up to 10 %), biotite, and sparsely aegirine-augite. Along the contacts of the alkaline granite with carbonatites and alkaline pyroxenites, hybrid rocks with a lepidogranoblastic texture, consisting of pyroxene, less often richterite, biotite, titanite, and microcline occur. They also form nest-like clusters.

Fenites appear in exo- and endocontacts of the alkaline pyroxenite: these are represented by greenish-gray fine- to medium-grained rocks with massive, spotty, and banded textures. They contain microcline (20–35 %), aegirine (20–30 %), richterite (10–20 %), biotite (20–30 %), albite (10–20 %), titanite up to 10 %, apatite up to 10 %, calcite up to 10

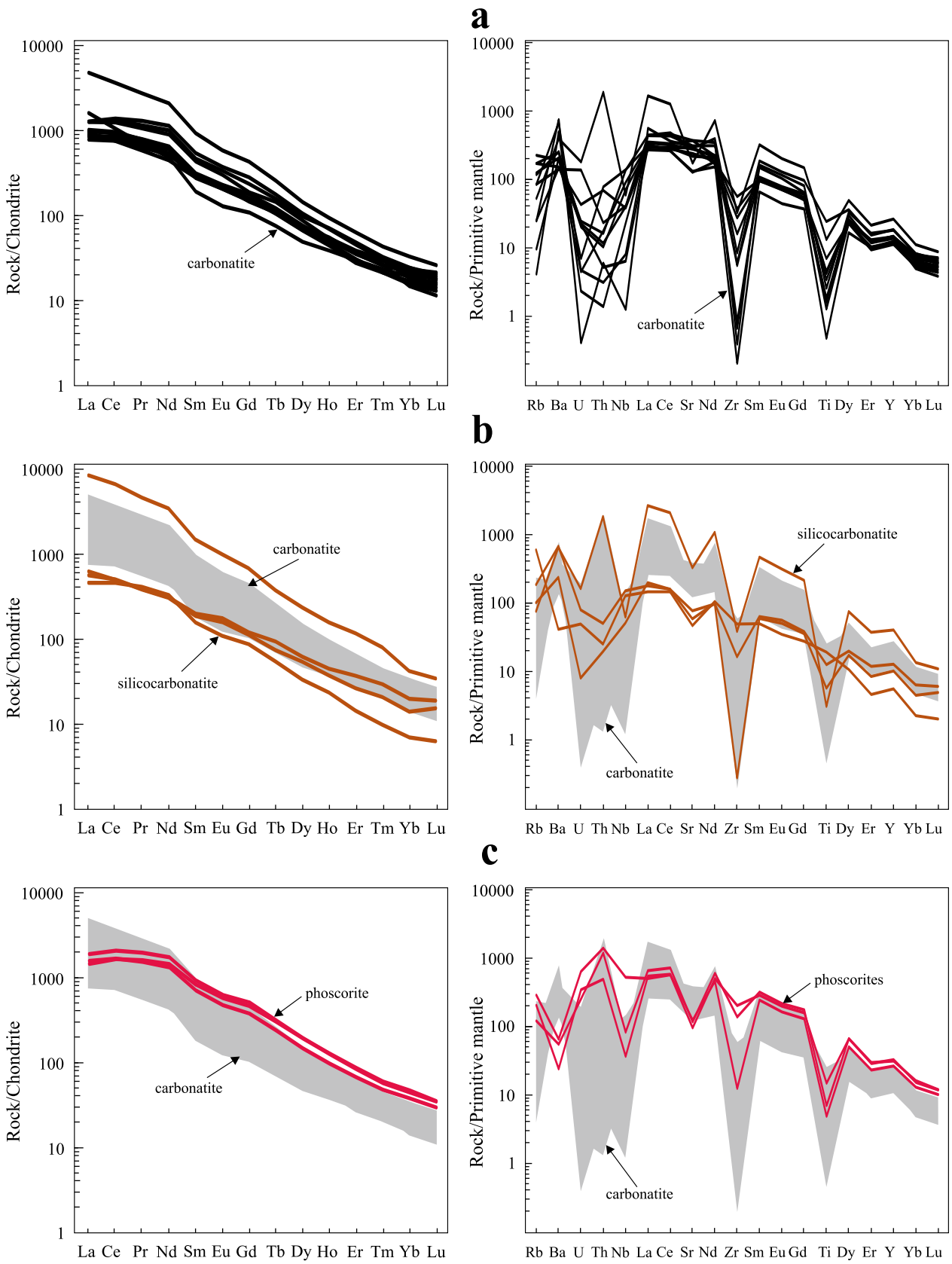

Fig. 3. Chondrite-normalized REE and PM-normalized trace element patterns: (a) the carbonatite, (b) the silicocarbonatite, (c) phoscorite; (d) the pyroxenite; (e) the syenite; (f) the alkali granite.

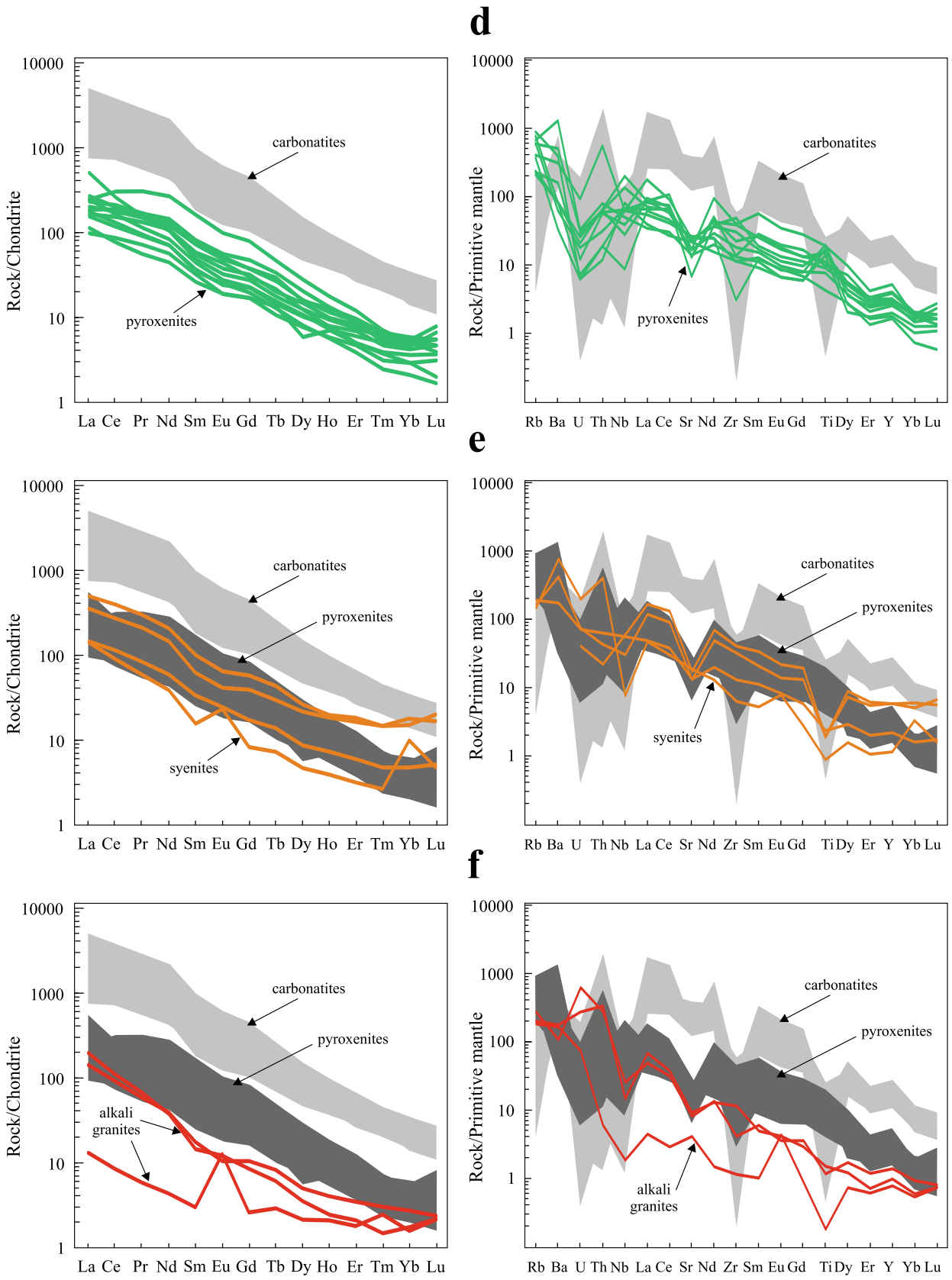

Fig. 3. (*continued*).

%.

4. Geochemistry

4.1. Carbonatites

The carbonatite contains CaO ranging 28.9–53.8 wt%. Loss on ignition, corresponding mainly to CO_2 content, varies 22.1–41.7 % (Supplementary Table 1). Amounts of the other major oxides change widely (SiO_2 = 0.7–15.2 wt%; TiO_2 = 0.5–4.2 wt%; FeO_{tot} = 0.8–18.0 wt %; MgO = 0.5–5.2 wt%; P_2O_5 = 0–4.0 wt%). Compared to the carbonatite, the CaO content in the silicocarbonatites decreases down to 15–25 wt%, while that of SiO_2 grows up (28.1–37.4 wt%).

The carbonatites and silicocarbonatites are enriched in trace and rare earth elements, whose contents vary very broadly: Sr = 671–3770 ppm, Ba = 1126–3280 ppm, ΣREE = 474–5710 ppm with a sharp predominance of LREE (La_N/Yb_N from 30 to 198) without obvious Eu anomalies (Eu/Eu* = 0.8–1.0). The HFSE contents are also highly changeable: Th = 4.6–171 ppm, Y = 30–139 ppm, Nb = 48–283 ppm, Ta = 0.7–9.6 ppm, Zr = 155–369 ppm, Hf = 3.9–8.2 ppm, but are generally comparable to an "average composition" of carbonatites (Chakhmouradian, 2006). Distribution of trace elements normalized to primitive mantle shows negative anomalies for Zr and Ti and positive anomalies for LREE (Fig. 3 a, b).

Due to the sparse occurrence of phoscorites, only four samples have been analyzed. However, these data obviously demonstrate their anomalous enrichment in phosphorus (P_2O_5 = 12.0–19.6 wt%) and iron (FeO_t = 19.1–25.3 wt%), as well as high field strength elements (Nb = 32–110 ppm, Y = 83–111 ppm, Zr = 431–1310 ppm, Th = 27–78 ppm, Ta = 3.6–15.0 ppm) and rare earth elements (∑REE = 1619–2133 ppm), with the same distribution pattern as in the carbonatite (Fig. 3 c).

4.2. Alkaline pyroxenites

Alkaline *pyroxenites of the Dubravinka massif* are distinguished by a wide concentration range of almost all petrogenic oxides: SiO_2 = 36.0–46.7 %, TiO_2 = 0.9–4.5 %, Al_2O_3 = 2.0–14.5 %, Fe_2O_{3tot} = 6.6–21.8 %, MgO = 2.7–11.7 %, CaO = 7.9–19.0 %, P_2O_5 = 0.02–1.71 % (Supplementary Table 1). The alkaline pyroxenites are low magnesian X_{Mg} = 32–58. Due to a high content of alkalis ($Na_2O + K_2O$ = 3.4–14.1 %) and sharp predominance of potassium over sodium, the alkaline pyroxenite compositionally correspond to alkaline picrites and foidites in the TAS diagram (Fig. 4 a), although they contain no normative nepheline.

The alkaline pyroxenite show very variable contents of iron group elements: low Cr (3–107 ppm, av. 21 ppm) and Ni (4–143 ppm, av. 64 ppm) and elevated V (55–682 ppm, av. 270 ppm) (Supplementary Table 1). High concentrations of lithophile elements: Sc (6–101 ppm, av. 46 ppm), Rb (129–543 ppm, av. 325 ppm), Sr (142–545 ppm, av. 362 ppm) and especially Ba (330–8744 ppm, av. 1922 ppm) also demonstrate significant variations. Of the HFSE, anomalously high contents of Nb (6–138 ppm, av. 47), slightly elevated Zr (34–535 ppm, av. 227 ppm) and Y (7–23 ppm, av. 13 ppm) were found. Concentrations of rare earth elements are also elevated (ΣREE = 123–458 ppm, av. 242 ppm) with intense fractionation and dominance of LREE (La_N/Yb_N = 27–83) without obvious Eu anomalies (Eu/Eu* = 0.8–1.0) (Fig. 3 d). Spider diagrams normalized to the primitive mantle display negative Zr, U and Sr anomalies and positive ones for Rb and LREE (Fig. 3 d).

Alkaline *pyroxenites of the Chernyanka massif* are more carbonatized and contain less biotite. They differ from the Dubravinka massif alkaline pyroxenites by a weak variability of main petrogenic oxides, low concentration of TiO_2 (1–2 wt%), but most prominently, by high content and predominance of Na_2O in the total alkali (Na_2O = 3.0–4.2 wt%;

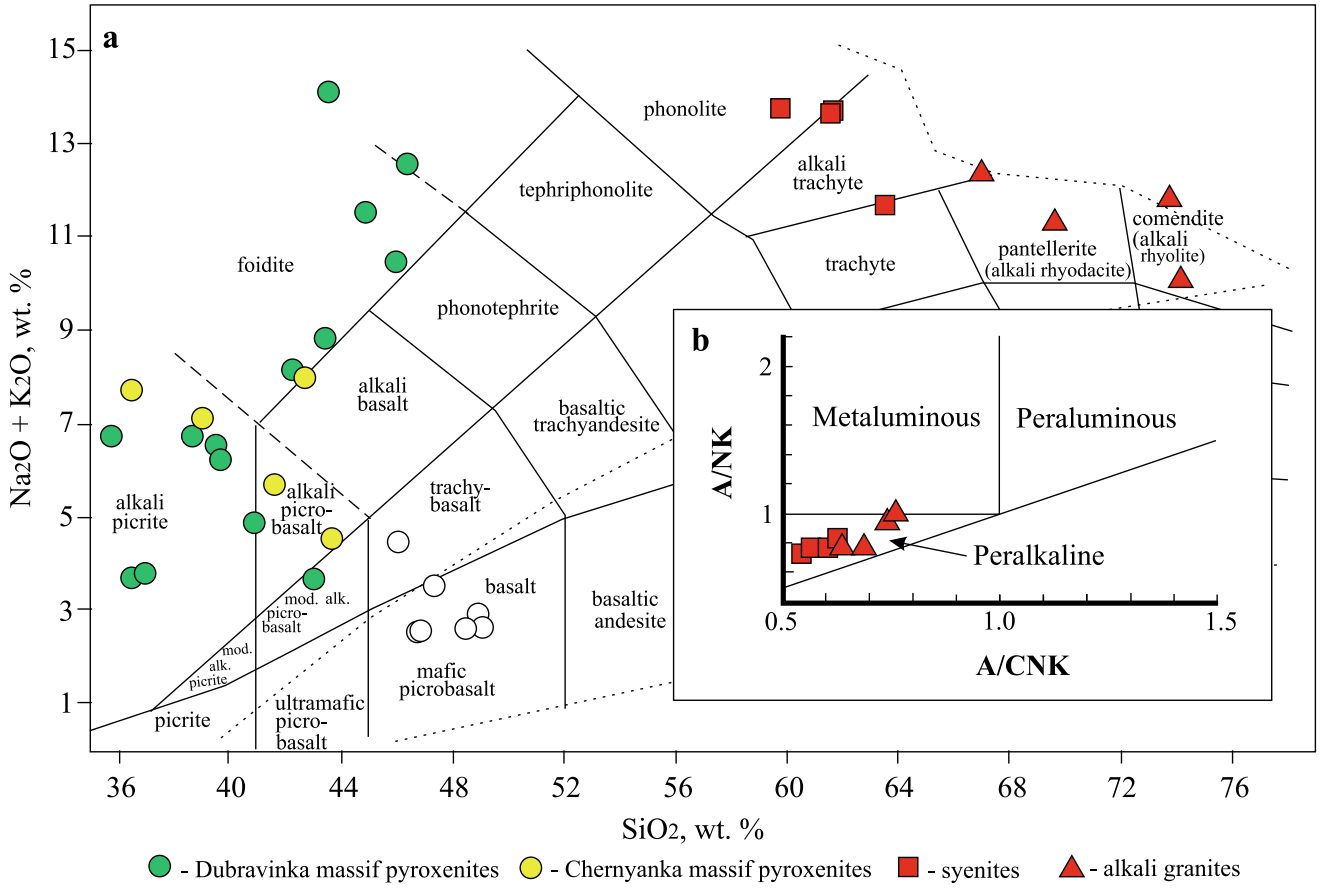

Fig. 4. The Dubravinsky ACC rocks on the classification diagrams (a) after (Middlemost, 1994); (b) after (Maniar and Piccoli, 1989).

Na_2O/K_2O = 1.1–4.3) (Supplementary Table 1). They are also differing in the distribution of trace elements. On average, there is less vanadium (116–246 ppm, av. 186 ppm), but twice as much of Ni (63–197 ppm, av. 122 ppm) and Cr (37–110 ppm, av. 74 ppm) in the Chernyanka massif alkaline pyroxenite. Of the lithophile elements, the content of Rb is three times lower (76–99 ppm, av. 84 ppm), but very high Sr (665–1535 ppm, av. 1009 ppm) at similar concentrations of Ba. They have anomalously high concentrations of Nb, but are depleted in Zr. There are also higher REE contents (423–695 ppm, av. 537 ppm) with almost the same distribution pattern.

4.3. Syenites and alkaline granites

Syenites with SiO_2 contents from 59.5 to 63.8 wt% have a very high iron content (X_{Fe} = 93–96, except for one analysis) and are enriched in alkalis ($Na_2O + K_2O$ = 11.1–13.6 wt%) with a significant predominance of potassium (K_2O/Na_2O = 2–4). They are characterized by high and moderate concentrations of lithophile and rare earth elements (Rb = 95–233 ppm, av. 133; Sr = 281–389 ppm, av. 334; Ba = 1220–5380 ppm; ΣREE = 118–520 ppm, av. 289) with LREE predominance (La_N/Yb_N = 23–71) without negative Eu anomalies (Fig. 3 e). The syenites may be divided into two groups according to HFSE and REE content. The first group (well 5450) differs by higher (more than twice) contents of Zr (364–460 ppm), Y (27 ppm), and REE (ΣREE = 364–520) from the second one (drillhole 5449) (Supplementary Table 1).

Alkaline granites have variable contents of SiO_2 (67–73 wt%) and high alkalis ($K_2O + Na_2O$ = 9.9–12.0 wt%) with a predominance of potassium over sodium (K_2O/Na_2O = 2.3–6.6) and calcium enrichment (CaO = 1.7–3.3 wt%). They have increased iron content (X_{Fe} = 68–85), but less than syenites. On the A/CNK diagram, the compositional points fall within the field of alkaline granites (Fig. 4 b). The granites are characterized by high contents of "mafic" elements (Cr and V), moderate Sr (88–197 ppm), Rb (128–173 ppm) and Ba (751–1160 ppm). Moderate concentrations of Nb (1.4–18.4 ppm), low concentrations of Y (3.6–6.4 ppm) and Zr (13–130 ppm) are recorded. Contents of rare earth elements are low (ΣREE less than 145 ppm), with the same distribution pattern as in the syenites (Fig. 3 f).

5. U-Pb ISOTOPIC AGE

Carbonatite. U-Pb isotopic age was determined on zircon from the silicocarbonatite (sample 1181/256) using SIMS SHRIMP-II. In addition, age of monazite from carbonatite was determined by ID TIMS (sample 891/403.2).

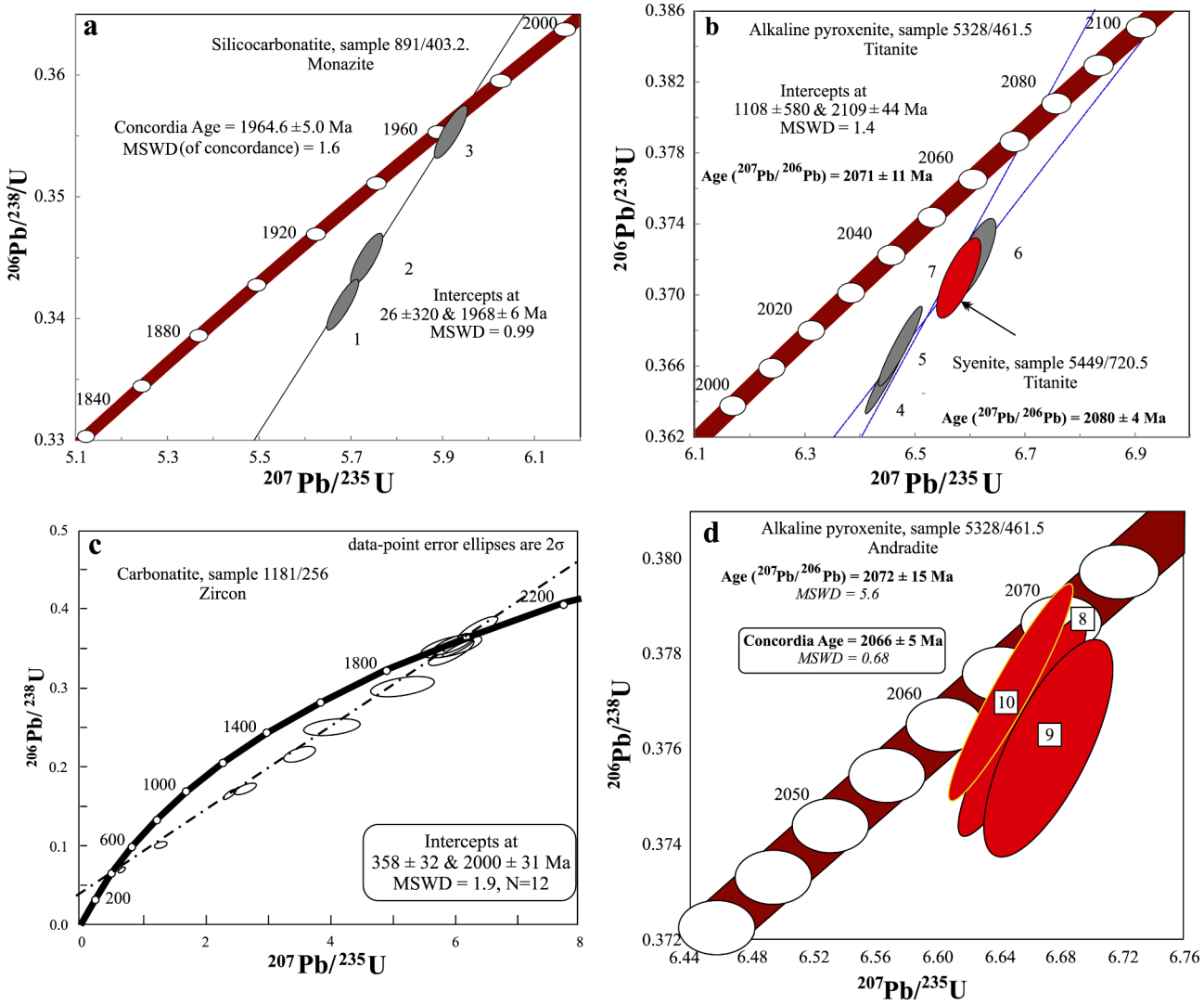

Fig. 5. The results of geochronological analyses (a) U-Pb ID-TIMS analyses of monazite from the silicocarbonatite; (b) U-Pb ID-TIMS analyses of titanite from the pyroxenite (sample 5328/461.5) and titanite from the syenite (sample 5449/720.5); (c) U-Pb SIMS analyses of zircons from the silicocarbonatite (sample 1181/256); (d) U-Pb ID-TIMS analyses of andradite from the pyroxenite.

Zircons in sample 1181/256 are euhedral and subhedral semi-transparent and transparent prismatic crystals of gray color, sometimes square in shape or with smoothed, almost rounded tips, 50–80 μm in size. In CL images, most crystals show a zonal structure – lighter inhomogeneous centers with patches of very dark high-uranium regions occupying up to 50 % area, and dark gray rims 10–15 μm as wide (Supplementary Fig. 4).

Totally 17 analyses have been done in 10 grains in the central parts and edges (Supplementary Fig. 4). The vast majority of results have a high degree of discordance (Supplementary Table 2), and only one, at 1959 ± 18 Ma, is concordant. The U-Pb isotope system in most of the grains is disturbed, which suggests influence of superimposed events. In the Ahrens-Wetherill diagram (Fig. 5 c) all the results approximate to a single regression line. The regression through all the results gives an upper intercept age of 2000 ± 31 Ma (MSWD = 1.9). Despite of some scatter the zircon is supposedly a single generation.

Lack of satisfactory result from U-Pb zircon dating prompted analysis of monazite. Three monazite fractions were analyzed (2–6 grains, size fraction > 100 μm, # 1–3, Supplementary Table 3) in the silicocarbonatite, sample 891/403.2. The data points of the analyzed fractions define a regression line with an upper intercept at 1965 ± 5 Ma (MSWD = 1.6) (Fig. 5 a, Supplementary Table 3).

Alkaline pyroxenite. Ages of titanite (sample 5328/461.5) and andradite (sample 5436/262.1) were determined by the U-Pb ID TIMS technique. Titanite forms large (>150 μm) fragments of semitransparent crystals of a dark brown color. The most transparent and free of gas and/or mineral inclusions crystals were selected for U-Pb isotope dating (# 4–6, Supplementary Table 3). Data points approximate by a discordia line with the upper intercept at 2109 ± 44 Ma (MSWD = 1.4 lower intercept is at 1108 ± 580 Ma). Averaged $^{207}Pb/^{206}Pb$ age of these titanite yielded 2071 ± 11 Ma (MSWD = 7.4) (Fig. 5 b).

Garnet in the alkaline pyroxenite (sample 5436/390.7) forms dark brown euhedral crystals c. 1 cm across. Some crystals intergrow with titanite. Garnet contains silica-salt inclusions (Supplementary Fig. 5) typical for minerals from alkaline and carbonatitic rocks (Panina and Motorina, 2008). The garnet composition ranges from $Adr_{74}Mrt_{1}Sch_{0.4}Grs_{0.1}$ to $Adr_{99}Mrt_{19}Sch_{5}Grs_{3}$. Some goldmanite (max 1.38 %), kimzeyite (max 1.33 %) and pyrope (max 1.33 %) components were also identified in this garnet.

Three garnet fractions were selected for U-Pb analysis. The results are presented in Supplementary Table 3 (# 8–10) and in the Concordia diagram (Fig. 5 d). The studied garnets have U content from 1.82 to 2.71 ppm, and low levels of common Pb (Pb_c/Pb_t = 0.05–0.31). The data points are located on the Concordia or slightly discordant (Fig. 5 d). Garnet from fraction No. 3 yielded a reasonable age of 2066 ± 5 Ma (MSWD = 0.68). The weighted average of $^{207}Pb/^{206}Pb$ ratios for all

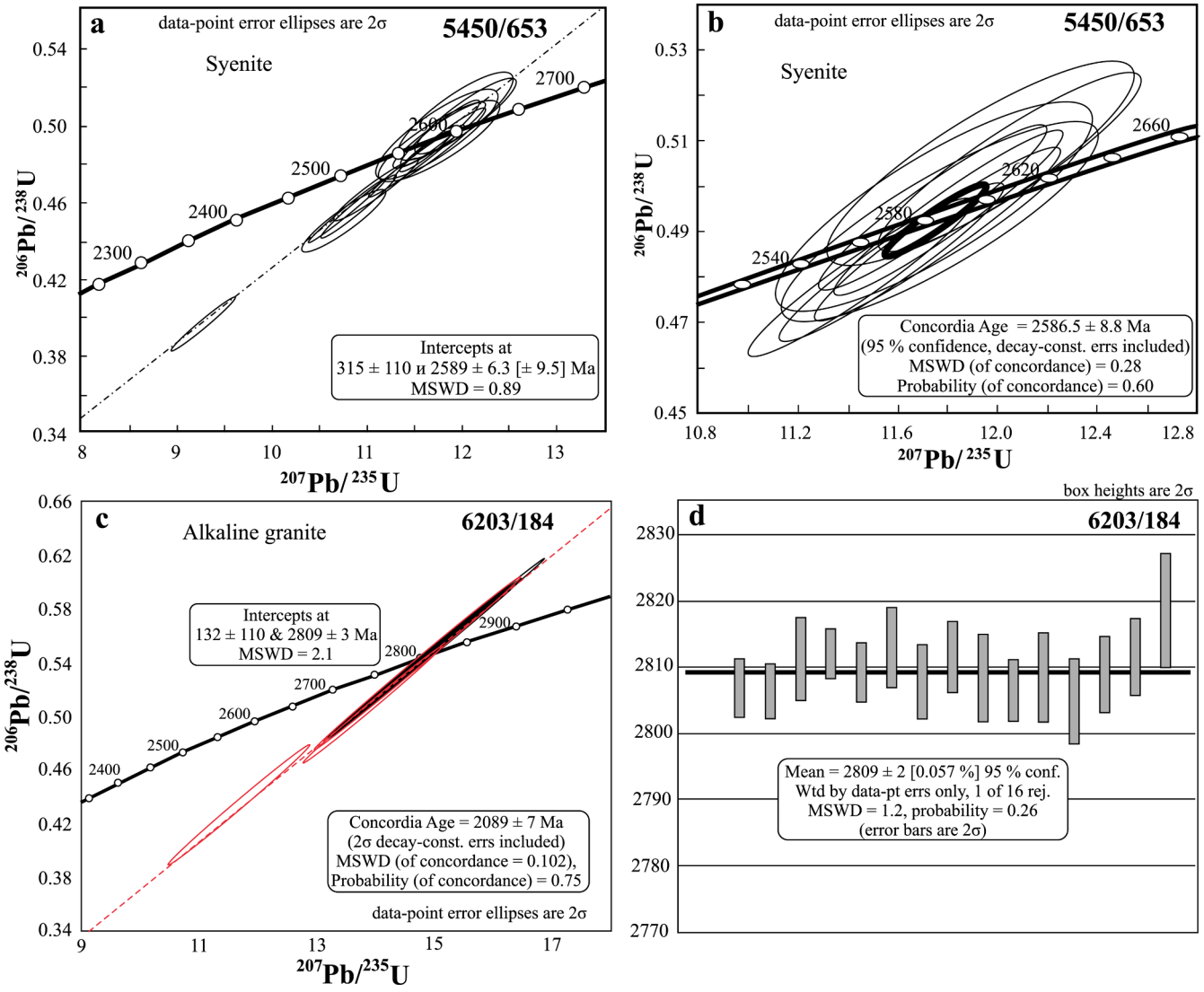

Fig. 6. The results of U-Pb SIMS analyses: (a, b) zircons from the syenite (sample 5450/653); (c, d) zircons from the alkaline granite (sample 6203/184).

studied fractions corresponds to an age of 2075 ± 15 Ma (MSWD = 5.6).

Syenite. Zircon in sample 5450/653 is represented by euhedral and subhedral elongated prismatic light brown crystals. Their length varies 150 to 500 μm, at 50–100 μm width. A fine rhythmic concentric oscillatory growth zoning in all zircon crystals is well pronounced in CL images. Non-zonal domains (possible recrystallization) are sometimes observed at their pyramidal terminations. Judging by the CL images, the early zircon phase is locally corroded prior to overgrowth by late zircon. There is one dark non-zoned short-prismatic grain (Supplementary Fig. 6).

Totally 15 analyses have been done in the 10 grains in the central and marginal parts using a SHRIMP-II ion microprobe (Supplementary Table 2). In the Ahrens-Wetherill diagram (Fig. 6 a, b) all the results approximate to a single regression line with the majority forming a concordant cluster. The low deviation of points from the regression line (MSWD = 0.89) assumes a minimal effect of the Precambrian processes on the zircons. These results coincide with the Concordia age (N = 9, MSWD = 0.13) of 2587 ± 9 Ma (Fig. 6 a, b). The only short prismatic grain has a subconcordant (D = 2) age of 2068 ± 6 Ma (point 3.1, Supplementary Table 2).

Titanite forms semitransparent light brown crystals. The most transparent five crystal fragments were used for U-Pb analysis. Titanite is slightly discordant (2 %) and yield $^{207}Pb/^{206}Pb$ age at 2080 ± 4 Ma; its data point locates directly on a discordia line constrained for titanite from the sample 5328/461.5 of alkaline pyroxenite (Fig. 5 b).

Alkaline granite. Zircons in sample 6203/184 are prismatic crystals with orbicular tips and rounded isometric grains and their brown fragments, transparent and semitransparent, 150–250 μm in size. In CL images, all grains are dark in color, zoning if any, obscured and have largely undergone metamictization due to the high content of U (1320–4130 ppm), which is well manifested in BSE-images (Supplementary Fig. 7).

Totally 15 analyses have been done in the 14 grains (Supplementary Fig. 7, Supplementary Table 2). In the Ahrens-Wetherill diagram all the results approximate to a single regression line. The regression through all the results gives an upper intercept age of 2809 ± 3 Ma (MSWD = 2.1, Fig. 6 c, d). The weighted average $^{207}Pb/^{206}Pb$ age of all results is 2809 ± 2 Ma (N = 15, MSWD = 1.2) (Fig. 6 c, d).

6. Isotope systematics

6.1. Sm-Nd isotopic data

In Sm-Nd isochronous coordinates, the alkali-carbonatite rocks demonstrate wide and irregular variations (Supplementary Table 4, Fig. 7). Only results from the alkaline granites (T c. 3.5 ± 1.6 Ga, MSWD = 5.5) and carbonatites (T c. 2.4 ± 0.9 Ga, MSWD = 13) show correlations close to linear (Fig. 8 a). However, large MSWD values and age uncertainties do not allow us to consider the lines as isochrones with any geological significance. The results from phoscorites, alkaline pyroxenites, and syenites display even greater scatter, thus providing no geochronological information. An inexplicably high value of εNd (2070 Ma) = +15.1 was obtained for a single sample of the silicocarbonatite.

6.2. Rb-Sr isotopic data

Analytical Rb-Sr results of the phoscorite and carbonatite sampled from a single body in the drillhole 5402 are approximate to a line with age of T c. 1.9 ± 0.3 Ga, MSWD = 44 (Fig. 8 b, c). The syenites produce a greater scatter aligning to a regression corresponding to value of T c. 1.9 ± 1.4 Ga (MSWD = 57) (Fig. 9 b). The carbonatite demonstrate the highest dispersion with no correlation (Fig. 8 c).

6.3. Lu-Hf isotopic data

The Hf isotope composition of the syenite zircons has been determined in the same points as the U-Pb age. Unlike the U-Pb isotope system, which gives similar ages (2589 ± 15 Ma) in all (but one) zircon grains, the Lu-Hf isotope system exhibits wide Hf variations with εHf (2589) = (-4.2) – (-11.9) (Fig. 9, Supplementary Table 5). The model ages THf(C) calculated by the two-stage model are mainly Paleoarchean from 3359 to 3817 Ma. A single zircon grain with an age of 2068 Ma εHf (2068) = (-12.7) yields a Paleoarchean model age THf(C) = 3501 Ma as well.

Similarly to Sm-Nd isotopy, isotope analysis of zircon from the silicocarbonatite, showed an unrealistically high radiogenic isotopic composition εHf(2000) = +7.5 – +22.8 and model ages younger than the age of their crystallization (Supplementary Table 5).

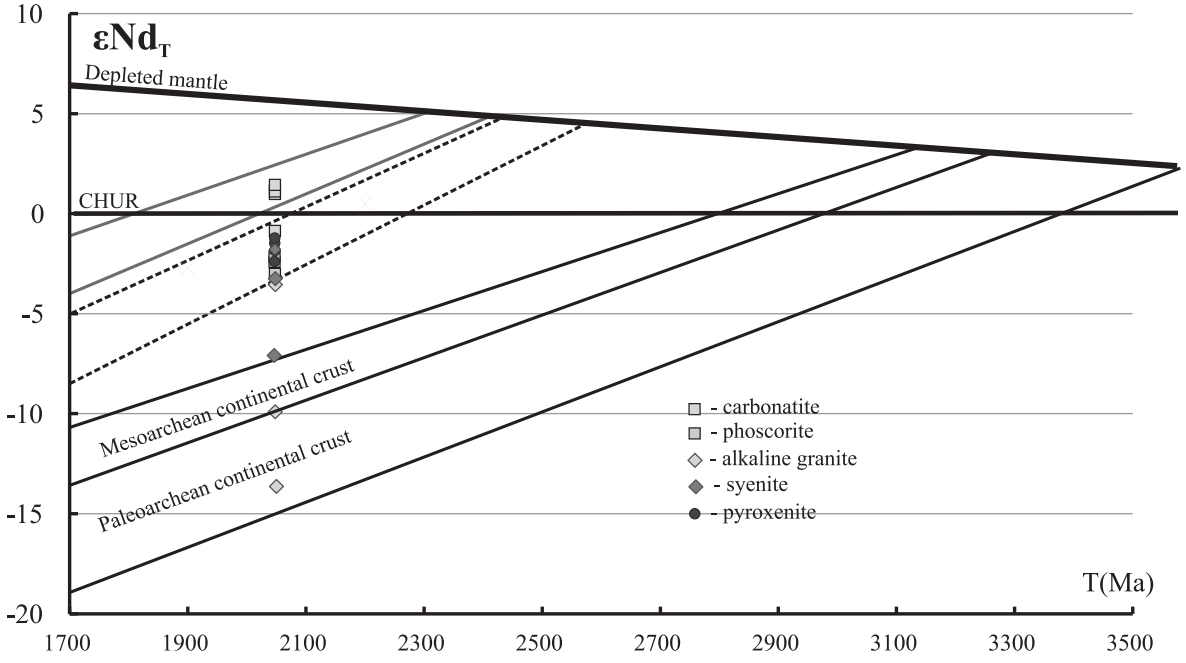

Fig. 7. Age–εNd(T) diagram for the Dubravinsky ACC rocks.

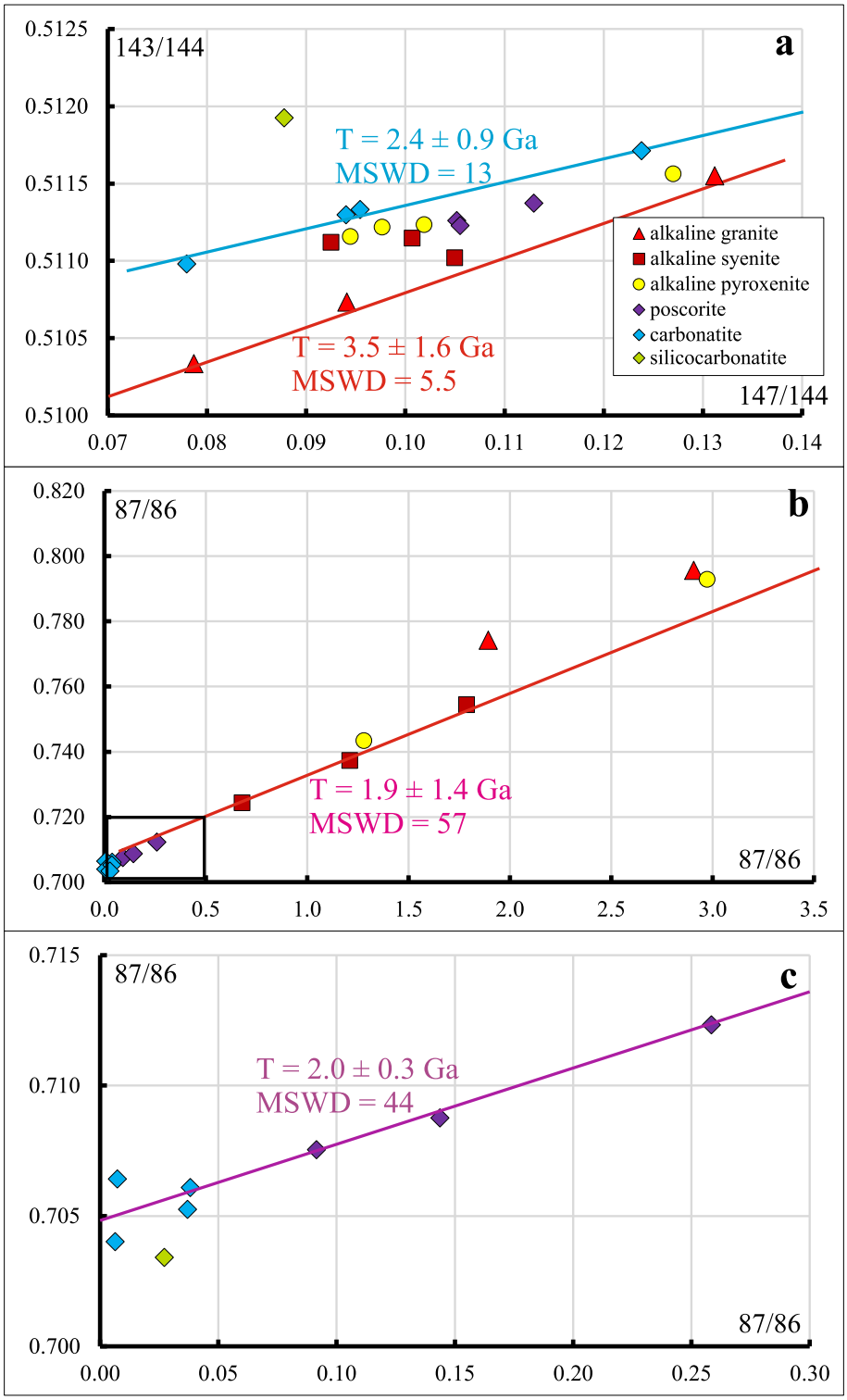

Fig. 8. Sm-Nd and Rb-Sr isochrones for the Dubravinsky ACC rocks.

6.4. C-O isotopic data

The isotope composition of carbon and oxygen was determined from bulk samples in the carbonatites and silicocarbonatites of the Dubravinka and Chernyanka intrusions. The $\delta^{13}C$ (‰ VPDB) values range narrowly from (-4.9) to (-6.4) and do not differ in the carbonatites and silicocarbonatites (Supplementary Table 6). Values of $\delta^{18}O$ (‰ VSMOW) also fall within a limited span (+8.0) – (+9.8) and being indistinguishable for the carbonatites and silicocarbonatites. Typically, isotope data for carbon and oxygen in carbonatite are compared to igneous carbonatite in the Primary Igneous Carbonatite (PIC) box. It is a rectangle in the $\delta^{13}C$ (‰ VPDB) – $\delta^{18}O$ (‰ VSMOW) diagram corresponding to isotope composition of a mantle source. Its boundaries have several versions (Deines 1989; Demény et al., 2004; Jones et al., 2013). We are guided by the PIC field (Demény et al., 2004) with the coordinates $\delta^{13}C$ (‰ VPDB) = (-4) – (-8) and $\delta^{18}O$ (‰ VSMOW) = +5.3 – +9.8. All values of carbon and oxygen isotope composition of the carbonatite and silicocarbonatite of the Dubravinsky complex fall within the region of

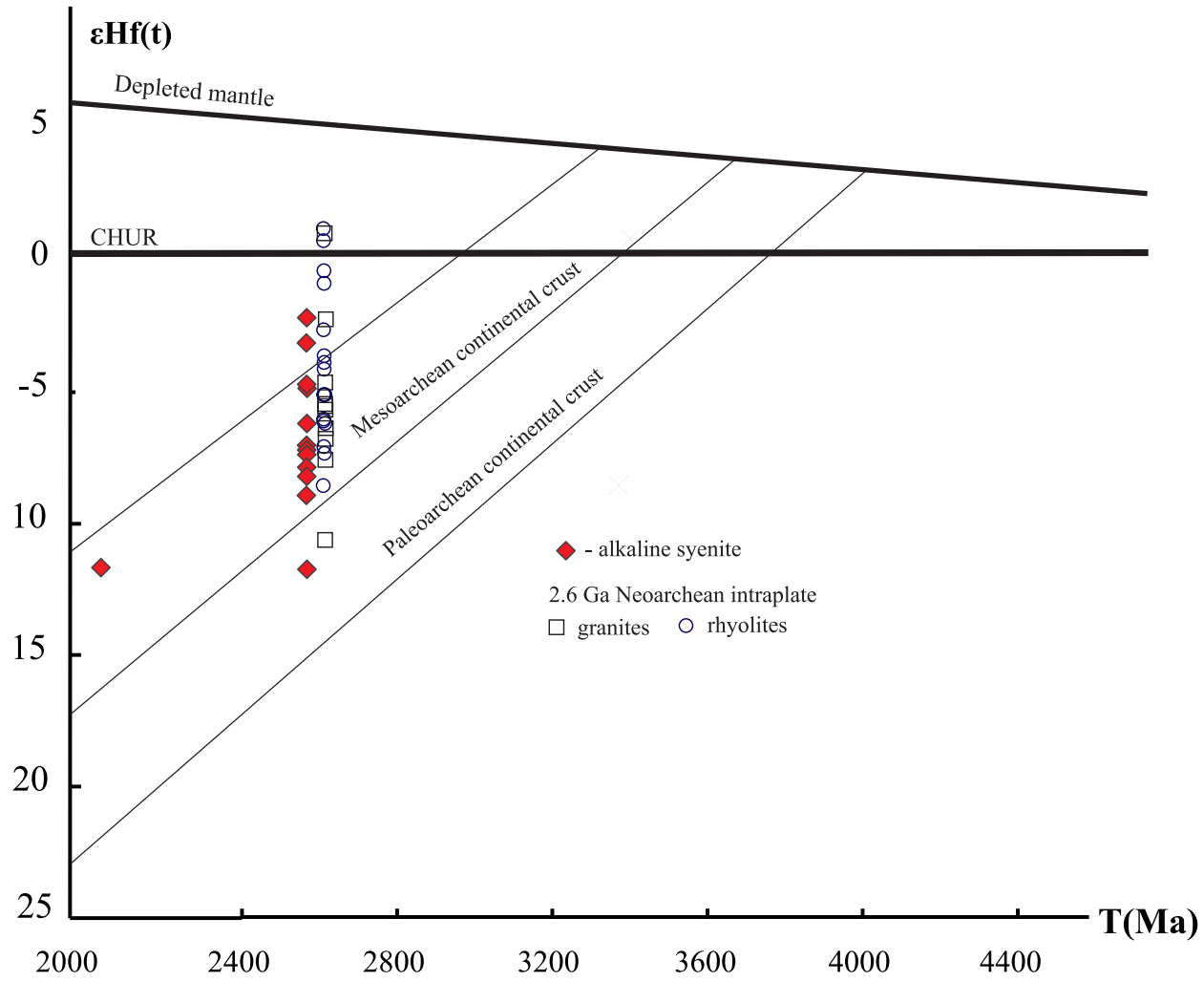

Fig. 9. Plots of εHf(t) values versus zircon ages for zircon grains from the syenite.

primary igneous carbonatites (Fig. 10).

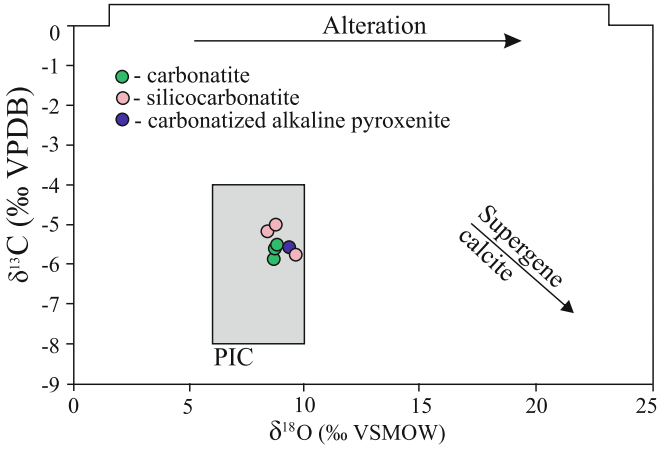

Fig. 10. Oxygen and carbon isotope ratios from the Dubravincky ACC carbonatite; PIC = primary igneous carbonatite box from (Demény et al., 2004).

7. Discussion

7.1. Regional correlations

The Dubravinsky alkaline-carbonatite complex is located within the Kursk-Besedino domain, which, together with the Azov block, forms the Paleoarchean core of eastern Sarmatia (Azov-Kursk domain) (Bogdanova et al., 2016; Savko et al., 2021a). In the Azov block of the Ukrainian Shield, the linear shape Chernigiv carbonatite complex is known (Glevasskiy and Kridvik, 1981): it resembles the Chernyanka intrusion. It is distinguished by a wide variety of rocks, including sevites, beforsites, alvikites, nepheline syenites, alkaline pyroxenites, and ijolite-melteigites. Zircon from the carbonatites yielded an age of 2074 ± 6 Ma, accepted their crystallization age (Rukhlov, Bell, 2010). The ages of apatite from the same sample are 2007 ± 1 and 1988 ± 2 Ma: this interpreted as the result of superimposed metamorphism or metasomatism (Rukhlov and Bell, 2010). Recent, U-Pb LA-ICP-MS dating of zircon from the nepheline syenites and carbonatites gave the same ages of 2072 ± 9 Ma (Shumlyanskyy et al., 2021). The carbonatites of the Chernigivka massif, as well as those of the Dubravinka massif have "mantle" values of stable ($\delta^{13}C$ from −3.8 to −8.6‰ V-PDB and $\delta^{18}O$ from + 5.0 to + 17.5 ‰ SMOW) and radiogenic values of εNd(2100) = +0.9 – +2.2; and $^{87}Sr/^{86}Sr(2100)$ = 0.70190–0.70156) (Dubyna et al., 2018; Zagnitko and Lugovaya, 1989).

The zircon age of 2.07–2.08 Ga of the Chernigiv carbonatite complex coincides with the age of titanite and garnet from the Dubravinsky

alkaline pyroxenites and carbonatites, while the c. 2.0 Ga apatite age corresponds to the age of monazite and zircon from the carbonatites. Thus, the carbonatite complexes have a close geological history in the Paleoproterozoic.

Taking into account that the Dubravinsky and Chernigiv complexes of alkaline rocks and carbonatites are located in the Paleoarchean Azov-Kursk domain, have the same age and mantle isotope-geochemical characteristics, they can be considered as a Paleoproterozoic alkaline-carbonatite province.

7.2. Metamorphism of the Dubravinsky ACC

The arched shape of the intrusive bodies of the Dubravinka massif suggests that they either have undergone metamorphism or injected a weak zone in an already folded structure. The 2.07 Ga HT/LP metamorphism has affected all the Paleoproterozoic structures of the Eastern Sarmatia. It was caused by collision of the Volga-Uralia segment and Sarmatia. The thermal source of collisional metamorphism in the Kursk block was heating during ductile folding (Savko et al., 2018). The pressures and temperatures of the metamorphism increase eastwards towards the boundary of the Kursk block with the Paleoproterozoic Volga-Don orogen from the upper greenschist facies to granulite facies.

The Kursk block had a "cold" continental lithosphere. According to their physical properties, the constituent rocks are very heterogeneous and can be divided into two main types: (1) the Archean migmatite-gneiss and granite and (2) the volcano-sedimentary rocks infilling Paleoproterozoic structures.

During the collision of Volga-Uralia and Sarmatia under conditions of unilateral stress directed from east to west (in present-day coordinates), solid and brittle Archean gneisses and granitoids being subjected to high-temperature conditions at 2.82 Ga did not underwent any metamorphic changes (Savko et al., 2018). Because of the rocks' low competence, high pressure causes rocks to fracture and shear but not to fold. In the Paleoproterozoic structures oriented parallel to the boundaries of the Volga-Don orogen, directed stress has caused ductile deformation of plastic sediments turning them into shales. The deformations are maximal at the structures sides where the BIF rocks occur plunging steeply.

Apparently before the collision, the Dubravinka massif was a steeply dipping linear body oriented in the sublatitudinal direction (in present-day coordinates) parallel (or obliquely) to the stress direction. As a result of the collision, a steeply dipping arc-shaped body of the Dubravinka alkaline-carbonatite massif was formed. Northerly the metabasite bodies have the same arched shapes, and the Dubravinka massif repeats the outlines of the northern closure of the Volotovo structure (Fig. 2 a). Unlike it, the Chernyanka massif, elongated in the meridional direction perpendicular to the direction of stress, did not change its orientation, but was probably flattened with a decrease in the width.

The carbonatites and carbonatized pyroxenites of the Dubravinka massif, located between the Tim-Yastrebovka and Volotovo Paleoproterozoic structures (Fig. 2 a), are too competent rocks to form a folded structure. They are characterized by granoblastic, lepidogranoblastic structures, sometimes gneissic and banded textures. In less competent syenites and alkaline granites, like Archean granitoids, with the exception of sparsely occurring directive textures, signs of superimposed metamorphism have not been found.

The P-T conditions of metamorphism of 630 °C and 4–5 kbar were estimated during a detailed study of metapelites and BIF of the Paleoproterozoic Prioskolskaya structure (Savko and Kal'mutskaya 2002), adjacent to the Chernyanka intrusion and 2 km west of the Dubravinka massif (Fig. 2 a).

7.3. Relationships of primary magmatic, postmagmatic and metamorphic characteristics

The alkaline pyroxenites and carbonatites are undoubtedly initially igneous rocks that have undergone high-temperature metamorphism. This is evidenced by: (1) the Dubravinka massif has the shape of a fold; (2) development of zones of biotite rocks (glimmerites) at the contact of the pyroxenites, carbonatites, and syenites; (3) dissemination, veinlets, lenticular segregations and injections of calcite in pyroxenites; (4) biotite-rimmed pyroxenite xenoliths in the carbonatite; (5) granoblastic and lepidogranoblastic structures and directive textures in the alkaline pyroxenite and carbonatite; (6) growth of a clearly superimposed microcline in the pyroxenite and carbonatite and absence of primary igneous olivine typical of foscorite from carbonatite complexes; (7) absence of chemical zoning in all minerals in the alkaline pyroxenite and carbonatite; (8) wide concentration variations of petrogenic oxides, trace and rare earth elements, due to very uneven distribution of microcline, calcite and biotite, as well as accessory minerals (magnetite, titanite, apatite, andradite) in them.

Presence of carbonate inclusions and injections in the alkaline pyroxenite and intrusive relationships between the alkaline pyroxenite and carbonatite indicate intrusion of new portions of carbonatite melt into the solidifying intrusive chamber. The syenite show almost no post-magmatic changes, with the exception of reaction zones at contacts with the carbonatite composed of alkaline amphibole, biotite with apatite, and sulfides. Discontinuous biotite-microcline zones and segregations with biotite rims are developed at contacts with the alkaline pyroxenite.

7.4. Interpretation of geochronological data

All the rock types in the alkaline-carbonatite complex occur in close spatial association, have alkalic compositions and have been formed by interrelated processes in the lower crust and mantle. This suggests the carbonatite intrusions and alkaline rocks age similarity. Based on geological, isotopic and geochemical data all of the Dubravinsky ACC rocks are thought to relate genetically to a single magmatic event.

U-Pb isotopic dating of zircon, titanite, monazite, and andradite yielded several age estimates that require reasonable interpretation.

1. Alkaline granite zircon is the oldest: its age of 2809 ± 3 Ma coincides with that of granulite metamorphism recorded in the Paleoarchean TTG, metapelites, and metabasites (Savko et al., 2018). The alkaline granites also have the lowest radiogenic Nd composition of all rocks and Archean model ages ($T_{Nd}DM$) (Fig. 7). These data, as well as the grains morphology imply that the c. 2.8 Ga zircon was entrained from the rocks of the Paleoarchean core of the Kursk block.

2. Zircon from the syenite has been dated to 2.59 Ga, and until new isotope-geochemical and geochronological data were obtained, it was erroneously interpreted as the age of intrusion of the Dubravinsky ACC. The Sr and Nd isotopic composition, recalculated to 2.59 Ga, in almost all samples fall out of range known for the Earth, suggesting more depleted magma sources than DM (Sm-Nd) and UR (Rb-Sr) (Fig. 11). This means that the value chosen for calculations is surfeits crystallization age of the alkaline syenite.

This suggests that zircon was inherited from a magma source with an age of about 2.6 Ga. Such sources of a kind are related to the 2.61 Ga intraplate magmatism of high-silica granitoids in the Kursk block (Savko et al., 2019). This interpretation can be confirmed by: (1) the dated alkaline syenite sample, in comparison with others, is sharply distinguished by the least radiogenic (crustal) neodymium isotope composition and, at the same time, by an anomalously high concentration of Zr; (2) the zircon morphology, dominated of long prismatic crystals, is not typical of alkaline rocks, where zircon has a short prismatic habit with hyacinth faceting; (3) the only short prismatic grain has an age of 2068 ± 6 Ma.

3. The ages of titanite 2071 ± 11 Ma and andradite 2075 ± 12 Ma from the alkaline pyroxenite, as well as of titanite from carbonatite 2080 ± 13 Ma (Albekov et al., 2017) and alkaline syenite 2080 ± 4 Ma coincide within the error with the age of HT/LP zonal metamorphism during the collision of Sarmatia and Volga-Uralia (Savko et al., 2018). Therefore, two interpretations of these ages are possible: (1) the age of

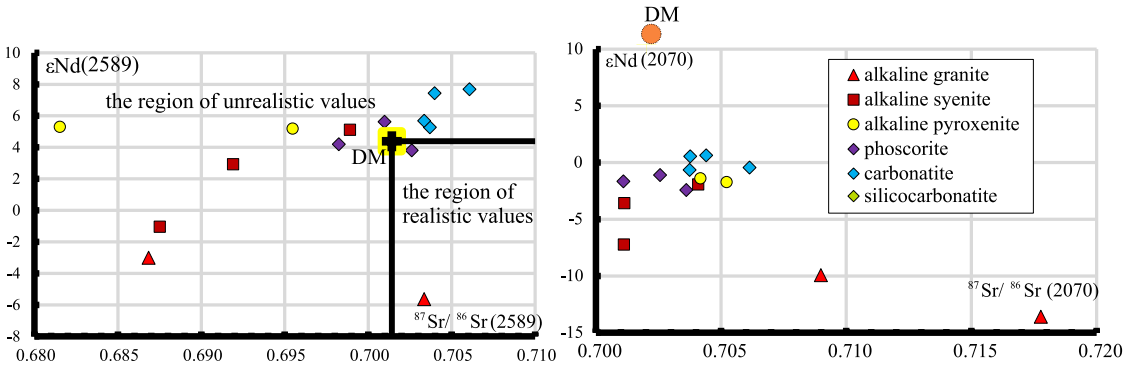

Fig. 11. εNd(t) – $^{87}Sr/^{86}Sr(T)$ diagram for the Dubravinsky ACC rocks, recalculated to 2589 and 2070 Ma.

the superimposed metamorphism and (2) the magmatic crystallization age is slightly older than the metamorphic event. The closing temperatures of the U-Pb titanite isotope system in the range of 650–700 °C (Frost et al., 2000) are close to the peak temperatures of metamorphism (c. 650 °C), precluding choosing one of interpretations. However, for calcium garnet with a grain size of 100 μm the closing temperature is 750–800 °C (Yang et al., 2018). This suggests that the U-Pb age of andradite from the alkaline pyroxenites of the Dubravinka massif corresponds to the age of their crystallization from the melt.

4. Zircon from the carbonatite has an age of 2000 ± 31 Ma. Monazite from carbonatite gave a younger age of 1965 ± 5 Ma. Rejecting the former due to a large uncertainty, latter is close to the age of zircon from the carbonatite and coincides with the only concordant value of 1959 ± 18 Ma. Apparently, these ages far postdate the peak of metamorphism at 2.07 Ga, thus rather correspond to a later activation during the collision of Sarmatia and the Osnitsko-Mikashevichi belt, recorded by a metamorphic event dated at c. 2.03 Ga (Savko et al., 2018) in the northwestern part of the Kursk block. Alternatively Pb-loss coincidentally could produce matching values.

Determination of the magmatic crystallization age of the carbonatite zircon should be done with great caution, since zircon may not be a primary magmatic mineral. It crystallizes from a carbonatite melt with a SiO_2 content of at least 20 wt% (Gervasoni et al., 2017; Rodionov et al., 2012). In addition, the Dubravinsky carbonatites underwent high-temperature metamorphism, which could lead to disturbance of isotope systems or new zircon growth.

Thus, the Dubravinsky ACC is most likely 2.07 Ga-old not much older than the metamorphic event. Here, we must take into account c. 2.07 Ga age of the Chernigiv ACC of the Ukrainian Shield (Rukhlov and Bell, 2010; Shumlyanskyy et al., 2021), which is located together with the Dubravinsky ACC within the Paleoarchean Azov-Kursk domain.

7.5. Isotope-geochemical data on the sources of melts

The wide variations of the Rb-Sr and Sm-Nd isotope results from individual rock types of the Dubravinsky ACC in the diagrams (Fig. 8) can be associated with heterogeneity of their igneous protoliths or caused by superimposed metamorphism. Most of the isotope-geochemical characteristics are probably features of igneous protoliths of the alkaline-carbonatite rocks, whose parental melts were derived from both crustal and mantle sources of different composition and age. The alkaline granites display well preserved isotope markers of a crustal source with a protracted Paleoarchean prehistory. The 2.8 Ga-old zircon in these rocks and negative εNd(T) values are likely inherited from an Archean crustal source (Fig. 7), matching well to a metamorphic zircon present in all types of host rocks of the Kursk–Besedino domain (Savko et al., 2021a). In the syenite, the Archean crustal component in the melt source is evidenced by the results of the U-Pb and Lu-Hf isotope analyses of zircon and Sm-Nd in the bulk sample of one of the analyzed samples. Two other samples of the syenite have a lesser contribution of Paleoarchean crustal material in terms of isotopic and geochemical characteristics.

Isotope-geochemical characteristics of the carbonatite, phoscorite, and alkaline pyroxenite indicate that their parental melts formed from a juvenile Paleoproterozoic mantle source. The carbonatite's mantle source is also clearly indicated by isotopic compositions of carbon and oxygen, all of which are within the mantle melts area (Fig. 10).

Neodymium isotope composition assumes that the carbonatite are more juvenile (εNd(2070) from (−0.8) to (+1.5) compared to the phoscorite (εNd(2070) from (−2.4) to (−3.3) and alkaline pyroxenite (εN(d2070) from (−1.4) to (−2.5) (Fig. 7; Supplementary Table 4). The lesser radiogenic neodymium isotope composition in the alkaline pyroxenite could be caused by impact of the syenite with crustal isotope characteristics, which is evident from petrographic data. Yet, the same explanation is inapplicable for the phoscorite, since they occur inside carbonatite bodies and bear no traces of the syenite influence. Moreover, it is extremely difficult to change the isotopic composition of neodymium in them due to very high concentrations of this element. The anomalously radiogenic isotopic composition of neodymium in the silicocarbonatite sample also remains unexplained. One can only assume that the unexplained variations of neodymium isotopic composition in essentially carbonate rocks were related to metamorphic impact. In general, by their Sr-Nd isotope-geochemical characteristics (Fig. 11), the rocks of the Dubravinsky ACC are close to their Phanerozoic counterparts (Hong et al., 2021).

After intrusion, the alkaline rocks and carbonatite experienced high-temperature metamorphism, which significantly increased hydrothermal activity, plasticity, and fluidity in carbonatites. Apparently, those conditions could cause the rock's partial melting and disturb isotope systems via subsolidus reactions between the U, Nd, and Hf concentrator-minerals (zircon, titanite, monazite) and a newly formed melt, consequently not always reflecting the primary intrusive isotope ratios. Partial or complete dissolution of these minerals and subsequent reprecipitation is a reason for redistribution of radiogenic elements between them and melt. Significant amounts of biotite and K-feldspar were formed in the alkaline carbonatized pyroxenites. Apparently, subsolidus processes and partial melting of the carbonatite during metamorphism also resulted in high heterogeneity of trace and rare earth elements contents. Disturbance of Rb-Sr, Sm-Nd (in rocks and minerals) and U-Pb (in zircon) isotope systems was recorded in the Early Precambrian carbonatite of Tishkeozero (1.98 Ga) and Siilinjärvi (2.61 Ga) as a result of the Svecofennian (1.9–1.7 Ga) metamorphism (Tichomirowa et al., 2006). Noteworthy, remobilization of U-Pb zircon isotopic system is observed in the carbonatites of the Grenville Province (1170 Ma) as a result c. 1080 Ma-old deformation and metamorphism (Moecher et al., 2011).

7.6. Petrogenetic and tectonic implications

The age of the Dubravinsky ACC of c. 2.07–2.08 Ga coincides within

the error with the age of metamorphism caused by collision of the Volga-Uralia and Sarmatia (Savko et al., 2018). In the period of 2.5–2.1 Ga, pulses of magmatism are not known in the Kursk block. A new burst of endogenous activity begins with basaltic 2099 ± 8 Ma-old magmatism related to asthenospheric melts upwelling in a destruction zone of a subducted oceanic slab (slab window) (Fig. 12 a, b). The cause of the slab detachment was an accretionary-collisional process of volcanic arc-continent type at the Kursk block margin and the Volga-Don orogen at about 2100 Ma (Tsybulyaev et al., 2021). After 2.1 Ga, there was a short post-collision period of relaxation during c. 2.08–2.07 Ga, when the rocks of the Dubravinsky ACC intruded (Fig. 12 c).

The source for the alkaline pyroxenites and carbonatites could be enriched protoliths from the subcontinental lithospheric mantle, produced by melting and release of fluids from the subducted oceanic slab at c. 2.1 Ga. Similar subduction-related enrichment of the subcontinental lithospheric mantle in the Paleoproterozoic was suggested for other parts of the craton (Konopelko and Eklund, 2003). Since the Kursk block was a passive continental margin prior to subduction, the enrichment of the mantle source occurred rapidly, within 10–15 Ma. After the continent–island arc collision and slab detachment, post-collision extension and the alkaline carbonatite magmatism took place in the interval of 2.07–2.08 Ga. The alkaline granites and some syenites are derivatives of crustal melting resulted from interaction with rising alkaline-ultramafic and carbonatite magmas. Thus, the intrusion of 2.08–2.07 Ga alkaline rocks and carbonatites is the result of magmatism in a suprasubduction setting with mantle and crustal sources (Fig. 12 c).

Later, about 2.07 Ga, a much larger continent–continent collision of Volga-Uralia and Sarmatia has involved, the Dubravinsky ACC rocks in a compression setting leading to deformation and metamorphism under conditions of high-temperature amphibolite facies (Fig. 12 d). After the completion of the continent–continent collision and the transition from compression to extension tectonics, they could again undergo thermal reworking as a result of widespread post-collision magmatism with an age of 2.07–2.05 Ga.

7.7. The Paleoproterozoic Dubravinsky carbonatite complex as the first sign of transition to deep steep subduction of the modern style

Prior to 2 Ga the carbonatite magmatism was very sporadic, with less than 10 of >600 carbonatite bodies known (Woolley and Kjarsgaard, 2008). The oldest well studied carbinatites are Tupertalik (3.0 Ga), Siilinjarvi (2.6 Ga), Hogenakkal (2.40 Ga), Palaborwa (2.06 Ga), Mt Weld (c. 2.06 Ga), Tiksheozero (1.99 Ga) (Bizzarro et al., 2002; Tichomirowa et al., 2006; Pandit et al., 2016; Wu et al., 2011; Zhukova et al., 2021; Sharkov et al., 2021) were formed in the intraplate setting under the influence of mantle plumes (Rukhlov and Bell, 2010). The global compilation shows that carbonatites begun to expand in the Late Proterozoic and thrive in the Phanerozoic (Liu et al., 2023; Yaxley et al., 2022).

The carbonatite formation prerequisite is the subcontinental lithoshperic mantle (SCLM) enrichment with carbon and other volatiles. Carbon does not have to be entirely derived from the subducted crust, but subduction contributes to it because primary mantle carbon alone was insufficient to form carbonatites after c. 3 Ga (Dasgupta, 2013). Subduction is possible even in the Archean at a mantle temperature (Tp) 170–200 °C higher than the modern one (Liu et al., 2023). However, under such conditions, the slabs will be hotter by 87–100 °C (1/2 Tp) than modern subduction zones, thus leaving nearly all crustal carbon of the subducting slab at shallow (e.g. subarc) depths (Dasgupta, 2013). In contrast, at the contemporary lower temperatures plates became more rigid, turning an oblique Archean underthrust into deep steep subduction and introducing abundant volatiles (c. 75 % of carbon) to deeper SCLM horizons (Plank and Manning, 2019). In addition, the mantle cooling promotes deep subduction, and volatiles are more likely to migrate and accumulate in the cold, thick, and refractory cratonic lithosphere (Sun and Dasgupta, 2019). Thus, both tectonics (i.e., subduction) and the thermal state of the mantle (i.e., cooling) influenced carbonatite magmatism over time. The increase of carbonatites does not mean that they are directly related to the modern type subduction zone, taking into account the different forms and time scales of carbon transport in the mantle (Farsang et al., 2021; Sun and Dasgupta, 2019). This is most likely the result of a rising influx of volatiles into the SCLM as a result of ascending magma flows caused by increased subduction rate and favorable physicochemical conditions in the SCLM. Subduction is responsible for the general enrichment of the SCLM, which subsequently, sometimes after tens and hundreds of millions of years, produces carbonatite magmas under effect of a plume, postcollision, and other geodynamic mechanisms. During the Archean and most of the Paleoproterozoic, with hotter mantle and no deep subduction to deliver volatiles, carbonatites were rare (Liu et al., 2023). But as the mantle cooled down, and subduction conveyed more volatiles into the colder mantle, carbonatites became more common, especially after c. 1 Ga. Thus, it is the subduction plays a crucial role in carbonatite formation.

In this context, the well-documented Dubravinsky 2.07 Ga-old carbonatite complex is the earliest formed by modern style tectonics, comprising subduction (2.17–2.10 Ga), arc-continent collision (2.10–2.08 Ga) and post-collision extension (2.08–2.07 Ga). It is the first sign of the deep steep subduction on the Earth in the Paleoproterozoic. Over time, suprasubduction post-collision carbonatites have become increasingly prominent alongside intraplate ones (Goodenough et al., 2021) due to increasingly active modern-style subduction tectonics.

8. Conclusions

1. The Dubravinsky ACC rocks include three main lithologies alkaline pyroxenites, carbonatites (together with silicocarbonatites and phoscorites) and syenites (including alkaline granites).
2. The alkaline pyroxenites and carbonatites are undoubtedly initially igneous rocks that have undergone 2.07 Ga-old high-grade metamorphism (>630 °C, 5 kbar).
3. The Dubravinsky ACC is most likely 2.07–2.08 Ga-old not much older than the metamorphic event.
4. The source for the alkaline pyroxenites and carbonatites could be enriched protoliths from the subcontinental lithospheric mantle, produced by melting and release of fluids from the subducted oceanic slab at c. 2.1 Ga. The primary igneous C and O isotope composition is preserved in the carbonatite. The alkaline granites display well preserved isotope markers of a long-lasting crustal prehistory with Paleoarchean sources. The syenites have a lesser contribution of Paleoarchean crustal material and are closer to a group of “mantle rocks”.
5. The Dubravinsky and Chernigiv complexes of alkaline rocks and carbonatites are located in the Paleoarchean Azov-Kursk domain, have the same age and mantle isotope-geochemical characteristics, therefore, they can be considered as a Paleoproterozoic alkaline-carbonatite province of Sarmatia.
6. The Dubravinsky ACC intrusion of 2.07–2.08 Ga is the result of magmatism in a suprasubduction setting with mantle and crustal sources. It is the earliest known, formed as a result of subduction-collision processes, and the first sign of transition to deep subduction in the modern style.

CRediT authorship contribution statement

Konstantin A. Savko: Conceptualization, Methodology, Investigation, Resources, Writing – original draft, Writing – review & editing, Visualization, Supervision, Funding acquisition, Project administration. **Alexander V. Samsonov:** Conceptualization, Methodology, Resources, Writing – original draft, Visualization, Supervision. **Ekaterina B. Salnikova:** Methodology, Software, Formal analysis, Writing – original draft, Writing – review & editing, Visualization. **Maria V. Stifeeva:**

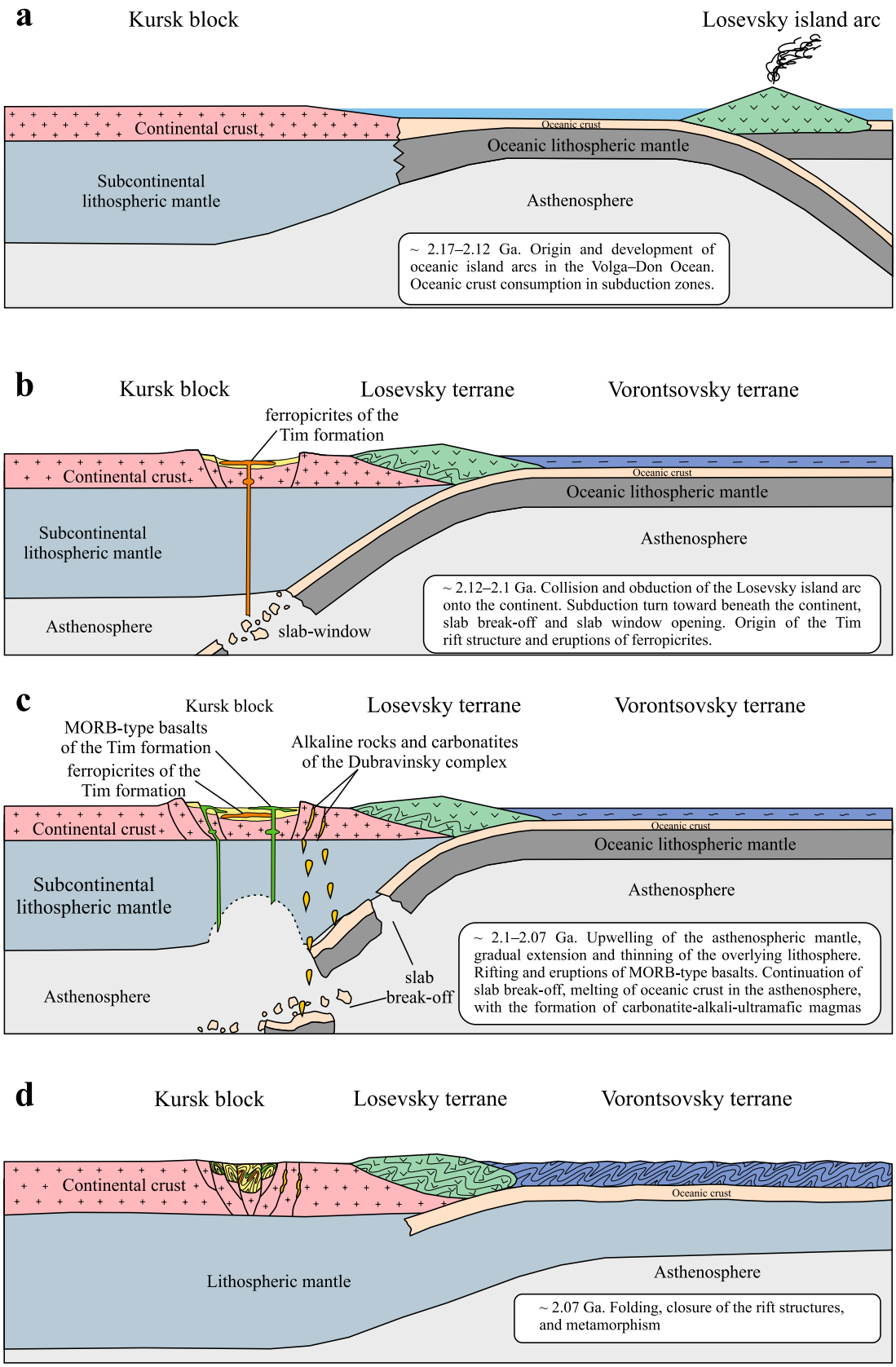

Fig. 12. Schematic illustration showing the tectono-magmatic processes for the Eastern margin of Sarmatia during c. 2.17–2.07 Ga.

Methodology, Software, Writing – original draft, Visualization. **Anton B. Kuznetsov:** Methodology, Software, Visualization. **Alexander B. Kotov:** Conceptualization, Methodology, Writing – review & editing, Visualization. **Yuliya O. Larionova:** Methodology, Formal analysis, Investigation. **Ekaterina H. Korish:** Methodology, Formal analysis, Investigation. **Alexander N. Larionov:** Methodology, Software, Formal analysis, Writing – original draft, Writing – review & editing, Visualization. **Mariya V. Chervyakovskaya:** Methodology, Software, Formal analysis, Visualization. **Sergey V. Tsybulyaev:** Validation, Data curation, Visualization. **Nikolay S. Bazikov:** Validation, Data curation, Writing – review & editing, Visualization.

Declaration of Competing Interest

The authors declare that they have no known competing financial interests or personal relationships that could have appeared to influence the work reported in this paper.

Data availability

Data will be made available on request.

Acknowledgements

This study was supported by the Russian Science Foundation, project no. 23-27-00007.

Appendix A. Supplementary material

Supplementary data to this article can be found online at https://doi.org/10.1016/j.precamres.2023.107153.

References

Albekov, A.Y., Chernyshov, N.M., Ryborak, M.V., Kuznetsov, V.S., Salnikova, E.B., Kholin, V.M., 2017. U-Pb isotopic age of apatite-bearing carbonatites in the Kursk Block. Voronezh Crystalline Massif. Dokl. Earth Sci. 473, 271–272. https://doi.org/10.1134/S1028334X17030205.

Bizzarro, M., Simonetti, A., Stevenson, R.K., David, J., 2002. Hf isotope evidence for a hidden mantle reservoir. Geology 30, 771–774. https://doi.org/10.1130/0091-7613(2002)030<0771:HIEFAH>2.0.CO;2.

Bogdanova, S.V., Gorbatschev, R., Garetsky, R.G., 2016. EUROPE|East European Craton. Reference Module in Earth Systems and Environmental Sciences, Elsevier. https://doi.org/10.1016/B978-0-12-409548-9.10020-X.

Chakhmouradian, A.R., 2006. High-field-strength elements in carbonatitic rocks: geochemistry, crystal chemistry and significance for constraining the sources of carbonatites. Chem. Geol. 235, 138–160. https://doi.org/10.1016/j.chemgeo.2006.06.008.

Dasgupta, R., 2013. Ingassing, storage, and outgassing of terrestrial carbon through geologic time. Rev. Mineral. Geochem. 75, 183–229. https://doi.org/10.2138/rmg.2013.75.7.

Deines, P., 1989. Stable isotope variations in carbonatite. In: Bell, K. (Ed.), Carbonatites: genesis and evolution. Unwin Hyman, London, pp. 301–359.

Demény, A., Sitnikova, M., Karchevsky, P., 2004. Stable C and O isotope compositions of carbonatite complexes of the Kola Alkaline Province: phoscorite–carbonatite relationships and source compositions. In: Wall, F., Zaitsev, A.N. (Eds.), Phoscorites and carbonatites from mantle to mine: the key example of the Kola Alkaline Province. The Mineralogical Society, London, pp. 407–431.

Dubyna, O.V., Kryvdik, S.G., Shumlyanskyy, L., Billström, K., Bekker, A., 2018. Trace elements geochemistry and isotope composition of the Chernihivka carbonatite complex, the Azov domain of the Ukrainian Shield. Geology and Mineral Resources of Ukraine, In., pp. 59–61

Farsang, S., Louvel, M., Zhao, C., Mezouar, M., Rosa, A.D., Widmer, R.N., Feng, X., Liu, J., Redfern, S.A., 2021. Deep carbon cycle constrained by carbonate solubility. Nat. Commun. 12, 4311. https://doi.org/10.1038/s41467-021-24533-7.

Frost, B.R., Chamberlain, K.R., Schumacher, J.C., 2000. Sphene (titanite): phase relations and role as a geochronometer. Chem. Geol. 172, 131–148. https://doi.org/10.1016/S0009-2541(00)00240-0.

Gervasoni, F., Klemme, S., Rohrbach, A., Grützner, T., Berndt, J., 2017. Experimental constraints on the stability of baddeleyite and zircon in carbonate- and silicate-carbonate melts. Am. Mineral. 102, 860–866. https://doi.org/10.2138/am-2017-5870.

Glevasskiy, E.B., Kridvik, S.G., 1981. Precambrian carbonatite complex of Azov region. USSR, Naukova Dumka, Kiev, p. 228 p. in Russian.

Goodenough, K.M., Deady, E.A., Beard, C.D., Broom-Fendley, S., Elliott, H.A.L., van den Berg, F., Öztürk, H., 2021. Carbonatites and Alkaline Igneous Rocks in Post-Collisional Settings: Storehouses of Rare Earth Elements. J. Earth Sci. 32 (6), 1332–1358. https://doi.org/10.1007/s12583-021-1500-5.

Gorbatschev, R., Bogdanova, S., 1993. Frontiers in the Baltic Shield. Precam. Res. 64, 3–21. https://doi.org/10.1016/0301-9268(93)90066-B.

Hong, J., Khan, T., Li, W., Khalil, Y.S., Narejo, A.A., Rashid, M.U., Zeb, M.J., 2021. SHRIMP U-Pb ages, mineralogy, and geochemistry of carbonatite–alkaline complexes of the Sillai Patti and Koga areas, NW Pakistan: Implications for petrogenesis and REE mineralization. Ore Geol. Rev. 139, 104547 https://doi.org/10.1016/j.oregeorev.2021.104547.

Hurai, V., Blažeková, M., Huraiová, M., Siegfried, P.R., Slobodník, M., Konečný, P., 2021. Thermobarometric and geochronologic constraints on the emplacement of the Neoproterozoic Evate carbonatite during exhumation of the Monapo granulite complex. Mozambique. Lithos 380–381, 105883. https://doi.org/10.1016/j.lithos.2020.105883.

Jones, A.P., Genge, M., Carmody, L., 2013. Carbonate melts and carbonatites. Rev. Mineral. Geochem. 75, 289–322. https://doi.org/10.2138/rmg.2013.75.10.

Konopelko, D., Eklund, O., 2003. Timing and geochemistry of potassic magmatism in the eastern part of the Svecofennian domain, NW Ladoga Lake Region, Russian Karelia. Precam. Res 120, 37–53. https://doi.org/10.1016/S0301-9268(02)00141-9.

Liu, S.-L., Ma, L., Zou, X., Fang, L., Qin, B., Melnik, A., Kirscher, U., Yang, K.-F., Fan, H. R., Mitchell, R.N., 2023. Trends and rhythms in carbonatites and kimberlites reflect thermo-tectonic evolution of Earth. Geology 51, 101–105. https://doi.org/10.1130/G50775.1.

Maniar, P.D., Piccoli, P.M., 1989. Tectonic discrimination of granitoids. Geol. Soc. Am. Bull. 101, 636–643. https://doi.org/10.1130/0016-7606(1989)101<0635:TDOG>2.3.CO;2.

Middlemost, E.A.K., 1994. Naming materials in the magma/igneous rock system. Earth Sci. Rev. 37, 215–224. https://doi.org/10.1016/0012-8252(94)90029-9.

Millonig, L.J., Gerdes, A., Groat, L.A., 2012. U-Th–Pb geochronology of meta-carbonatites and meta-alkaline rocks in the southern Canadian Cordillera: A geodynamic perspective. Lithos 152, 202–217. https://doi.org/10.1016/j.lithos.2012.06.016.

Moecher, D.P., Anderson, E.D., Cook, C.A., Mezger, K., 2011. The petrogenesis of metamorphosed carbonatites in the Grenville Province, Ontario. Can. J. Earth. Sci. 34 (9), 1185–1201. https://doi.org/10.1139/e17-095.

Monteiro, C.F., de Oliveira, I.L., Brod, J.A., Dantas, E.L., de Araujo, C.E.G., Zacchi, E.N. P., Fuck, R.A., 2020. Nd-Sr-Hf isotopes and U-Pb ages of mesoproterozoic Três Estradas Alkaline-Carbonatite Complex, Brazil: Implications for Sul-Riograndense Shield evolution and Rodinia break-up. Precam. Res. 351, 105963 https://doi.org/10.1016/j.precamres.2020.105963.

Pandit, M.K., Kumar, M., Sial, A.N., Sukumaran, G.B., Piementle, M., Ferreira, V.P., 2016. Geochemistry and C-O and Nd-Sr isotope characteristics of the 2.4 Ga Hogenakkal carbonatites from the South Indian Granulite Terrane: Evidence for an end-Archaean depleted component and mantle heterogeneity. Int. Geol. Rev. 58, 1461–1480. https://doi.org/10.1080/00206814.2016.1163646.

Panina, L.I., Motorina, I.V., 2008. Liquid immiscibility in deep-seated magmas and the generation of carbonatite melts. Geochem. Int. 46 (5), 448–464. https://doi.org/10.1134/S0016702908050029.

Pirajno, F., 2015. Intracontinental anorogenic alkaline magmatism and carbonatites associated mineral systems and the mantle plume connection. Gondw. Res. 27, 1181–1216. https://doi.org/10.1016/j.gr.2014.09.008.

Plank, T., Manning, C.E., 2019. Subducting carbon. Nature 574, 343–352. https://doi.org/10.1038/s41586-019-1643-z.

Rodionov, N.V., Belyatsky, B.V., Antonov, A.V., Kapitonov, I.N., Sergeev, S.A., 2012. Comparative in-situ U-Th-Pb geochronology and trace element composition of baddeleyite and low-U zircon from carbonatites of the Palaeozoic Kovdor alkaline-ultramafic complex, Kola Peninsula, Russia. Gondw. Res. 21, 728–744. https://doi.org/10.1016/j.gr.2011.10.005.

Rukhlov, A.S., Bell, K., 2010. Geochronology of carbonatites from the Canadian and Baltic Shields, and the Canadian Cordillera: clues to mantle evolution. Miner. Petrol. 98, 11–54. https://doi.org/10.1007/s00710-009-0054-5.

Savko, K.A., Samsonov, A.V., Kotov, A.B., Sal'nikova, E.B., Korish, E.H., Larionov, A.N., Anisimova, I.V., Bazikov, N.S., 2018. The Early Precambrian Metamorphic Events in Eastern Sarmatia. Precam. Res. 311, 1–23. https://doi.org/10.1016/j.precamres.2018.04.009.

Savko, K.A., Samsonov, A.V., Kholina, N.V., Larionov, A.N., Zaitseva, M.V., Korish, E.H., Bazikov, N.S., Terentiev, R.A., 2019. 2.6 Ga high-Si rhyolites and granites in the Kursk Domain, Eastern Sarmatia: Petrology and application for the Archean palaeocontinental correlations. Precam. Res. 322, 170–192. https://doi.org/10.1016/j.precamres.2019.01.006.

Savko, K.A., Samsonov, A.V., Larionov, A.N., Chervyakovskaya, M.V., Korish, E.H., Larionova, Y.O., Bazikov, N.S., Tsybulyaev, S.V., 2021a. A buried Paleoarchean core of the Eastern Sarmatia, Kursk block: U-Pb, Lu-Hf and Sm-Nd isotope mapping and paleotectonic application. Precam. Res. 353, 106021 https://doi.org/10.1016/j.precamres.2020.106021.

Savko, K.A., Samsonov, A.V., Santosh, M., Ovchinnikova, M.Y., 2021b. Neoarchean-Palaeoproterozoic sedimentary basins in the Sarmatian Craton: Global correlations and connections. Geol. J. 56 (3), 4479–4498. https://doi.org/10.1002/gj. 4185.

Savko, K.A., Kal'mutskaya, N.Yu., 2002. Petrology of potassium-poor metapelites of the Voronezh Crystalline Massif with reference to the olivine–gedrite–orthopyroxene–garnet–magnetite assemblage. Petrology 10 (3), 249–276.

Sharkov, E.V., Bogina, M.M., Shchiptsov, V.V., Belyatsky, B.V., Frolov, P.V., 2021. Petrology of the Mid-Paleoproterozoic Tiksheozero Ultramafic-Alkaline-Carbonatite Complex (Northern Karelia). Petrology 29 (5), 475–501. https://doi.org/10.1134/S0869591121050076.

Shumlyanskyy, L.V., Dubyna, O.V., Kryvdik, S.G., 2021. New Paleoproterozoic U-Pb ages for mafic-ultramafic and alkaline intrusions in the Ukrainian Shield. In: Developing the full potential of the large igneous province (LIP) record for multi-commodity, multi-scale exploration targeting at: Toronto. Ontario, Canada, pp. 55–56.

Sun, C., Dasgupta, R., 2019. Slab-mantle interaction, carbon transport, and kimberlite generation in the deep upper mantle. Earth Planet. Sci. Lett. 506, 38–52. https://doi.org/10.1016/j.epsl.2018.10.028.

Tichomirowa, M., Grosche, G., Gotze, J., Belyatsky, B.V., Savva, E.V., Keller, J., Todt, W., 2006. The mineral isotope composition of two Precambrian carbonatite complexes from the Kola Alkaline Province – Alteration versus primary magmatic signatures. Lithos 91, 229–249. https://doi.org/10.1016/j.lithos.2006.03.019.

Tsybulyaev, S.V., Savko, K.A., Samsonov, A.V., Korish, E.K., 2021. Paleoproterozoic OIB- and MORB-Type Rift Volcanics of the Kursk Block, Eastern Sarmatia: Petrology and Geodynamics. Petrology 29 (2), 114–147. https://doi.org/10.1134/S0869591121020065.

Woolley, A.R., Kjarsgaard, B.A., 2008. Paragenetic types of carbonatite as indicated by the diversity and relative abundances of associated silicate rocks: Evidence from a global database. Can. Mineral. 46, 741–752. https://doi.org/10.3749/canmin.46.4.741.

Wu, F.Y., Yang, Y.H., Li, Q.L., Mitchell, R.H., Dawson, J.B., Brandl, G., Yuhara, M., 2011. In situ determination of U-Pb ages and Sr-Nd-Hf isotopic constraints on the petrogenesis of the Phalaborwa carbonatite Complex, South Africa. Lithos 127, 309–322. https://doi.org/10.1016/j.lithos.2011.09.005.

Yang, Y.H., Wu, F.Y., Yang, J.H., Mitchell, R.H., Zhao, Z.F., Xie, L.W., Huang, C., Ma, Q., Yang, M., Zhao, H., 2018. U-Pb age determination of schorlomite garnet by laser ablation inductively coupled plasma Mass spectrometry. J. Anal. At. Spectrom 33, 231–239. https://doi.org/10.1039/C7JA00315C.

Yaxley, G.M., Anenburg, M., Tappe, S., Decree, S., Guzmics, T., 2022. Carbonatites: Classification, Sources, Evolution, and Emplacement. Annu. Rev. Earth Planet. Sci. 50, 261–293. https://doi.org/10.1146/annurev-earth-032320-104243.

Zagnitko, V.N., Lugovaya, I.P., 1989. Isotope geochemistry of carbonate and BIF of the Ukrainian Shield. USSR, Naukova Dumka, Kiev, p. 316 p. in Russian.

Zhukova, I.A., Stepanov, A.S., Jiang, S.-Y., Murphy, D., Mavrogenes, J., Allen, C., Chen, W., Bottrill, R., 2021. Complex REE systematics of carbonatites and weathering products from uniquely rich Mount Weld REE deposit, Western Australia. Ore Geol. Rev. 139, 104539 https://doi.org/10.1016/j.oregeorev.2021.104539.